AXIALLY GROOVED HEAT PIPE STUDY

JUNE, 1977

B&K ENGINEERING, INC.

BK012-1009

SUMMARY REPORT
FOR
AXIALLY GROOVED HEAT PIPE
STUDY

July 1977

Prepared for

NASA/Goddard Space Flight Center

Under

Contract No. NAS5-22562

Prepared by: H. Jen

Approved by: E. J. Kroliczek

B & K ENGINEERING, INC.

Suite 825, One Investment Place

Towson, Maryland 21204

SUMMARY

This report presents the results of a technology evaluation study on axially grooved heat pipes conducted under contract NAS5-22562. The state-of-the-art is reviewed and present and future requirements are identified. Analytical models which were developed under this program and parametric design studies which were conducted to evaluate potential performance improvements are also presented.

Analytical models include the Groove Analysis Program (GAP) and a closed form solution designed to facilitate parametric performance evaluations. GAP provides a numerical solution of the differential equations which govern the hydrodynamic flow. The model accounts for liquid recession, liquid/vapor shear interaction, 1-g puddle flow as well as laminar and turbulent vapor flow conditions. It can be used to obtain ideal charge and undercharge performance in both o-g and 1-g as well as the overcharge puddle flow contribution in 1-g. Good agreement between GAP predictions and measured data has been obtained with deviations noted only at high and low elevations and in the turbulent vapor flow regime.

The closed form solution was developed to reduce computation time and complexity in parametric evaluations. It is applicable to laminar and ideal charge conditions. Liquid/vapor shear interaction and an empirical liquid flow factor which accounts for groove geometry and liquid recession effects are included as part of the closed form solution. The validity of the closed form solution has been verified by comparison with GAP predictions and measured data.

Parametric analyses conducted with the closed form solution indicate that substantial performance improvements can be achieved. Care must be taken, however, to recognize the composite aspects of improved groove designs. A composite factor S has been defined which accounts for this effect.

An improved groove design which has a composite factor of 1.25 is defined. It's predicted transport capability is 75% higher and it has twice the static height than that provided by the current GSFC extrusion.

CONTENTS

ILLUSTRATIONS

Illustrations (Con't)

Illustrations (Con't)

TABLES

1.0 INTRODUCTION

Axially grooved heat pipe technology has been developed extensively for fixed conductance applications in the cryogenic through ambient temperature ranges. Aluminum axially grooved heat pipes flown aboard the Orbiting Astronomical Observatory-C (OAC) and the Applications Technology Satellite-6 (ATS-6) have demonstrated the reliability, versitility and cost effectiveness of this design. Recent developments include the adaptation of axially grooved tubing for use in thermal control heat pipes (TCHP) applications, the development of a copper/water axially grooved heat pipe for application up to 500°K and the fabrication of stainless steel axially grooved tubing for TCHP applications.

The advantage of the axially grooved heat pipe is that its internal configuration consists of a number of independent flow channels which are fabricated as an integral part of the tube wall and are parallel to its longitudinal axis. These channels develop the capillary pumping and offer low resistance to liquid flow. As a result the o-g heat transport capability of the axially grooved heat pipe is only exceeded by the more complex and less reliable composite wick designs. These channels, however, are also sensitive to elevation, puddle flow contributions in 1-g and the shearing effect of the vapor counterflow past the liquid. Each of these effects must be accounted for to accurately predict the performance. Analytical models are presented which incorporate these effects.

The models developed include the Groove Analysis Program (GAP) which solves the differential form of the governing hydrodynamic equations and a simplified closed form solution designed to facilitate parametric performance

evaluations. The validity of the models has been established by comparison of predicted values with measured data for various fluids and groove geometries.

The results of a technology evaluation study conducted under this contract are presented in this report. The analytical models developed together with comparisons with existing test data are also included. In addition, results of a parametric design analysis study which was conducted to determine potential groove geometry improvements is also discussed and an improved groove design is recommended.

2.0 TECHNOLOGY REVIEW

Axially grooved heat pipe technology has been developed extensively for fixed conductance applications in the cryogenic through ambient temperature range.[1,2] An aluminum axially grooved heat pipe flown aboard the Orbiting Astronomical Observatory-C (OAO-C)[3] is still functioning properly after more than four years in orbit. A total of 55 aluminum axially grooved heat pipes were also used to isothermalize the Applications Technology Satellite-6 (ATS-6).[4] Their extensive use and successful performance through almost three years of continuous flight operation has demonstrated the reliability of this design. Sounding Rocket Experiments[5,6] have also evaluated various performance parameters for these pipes.

Aluminum axially grooved heat pipes have been adapted for use as a gas controlled variable conductance (VCHP) system[7,8] within the past two years. Both feedback and passive VCHP control have been demonstrated in the 180-300°K range.[9,10] The feasibility of axially grooved diodes and thermal switches is also currently under investigation.[10] Finally, fabrication with materials other than aluminum to accomodate higher temperatures and different working fluids as well as low material conductance for thermal control applications is currently under investigation. A copper/water axially grooved heat pipe for use in the isothermalization of radiator fins of a radioisotope thermoelectric generator (RTG) has been developed and operated at temperatures up to 500°K.[11]

In short, the axially grooved heat pipe is being applied to a large variety of aerospace requirements. Potential terrestrial applications are also numerous and equally diversified. Typical performance requirements for various areas of application currently under consideration are summarized in the next section. Current state-of-the-art is also discussed and technology improvements which will serve to extend the usefulness of axially grooved heat pipes are identified.

2.1 Present and Future Requirements

Because there are many potential applications, heat pipe designs and performance requirements also tend to be many and varied. While it is difficult to quantify all of the requirements, some categorization can be developed to establish generalized criteria which can ultimately be used to establish standardized heat pipe designs. Heat pipe design and performance requirements fall into two general categories:

(1) Fixed conductance applications

(2) Thermal control applications

Within each of these categories, requirements are also dependent on the temperature range of application which can be classified as:

(a) Cryogenic to Low Temperature -- (0 - 250°K)

(b) Ambient -- (250 - 350°K)

(c) Intermediate to high temperature -- (>350°K)

A summary of the requirements for various applications which were determined from current and past flight programs and a survey of NASA and the aerospace industry is presented below.

2.1.1 Cryogenic Applications

A well defined need for a variety of cryogenic heat pipe hardware has been identified. Potential applications include passive heat pipe/radiant cooler systems and hybrid coolers such as the one illustrated in Fig. 2-1.[12,13] Such systems would be used to augment or replace present coolers in order to achieve longer life and lighter weight. The use of heat pipes to couple remote components to centrally located active coolers such as a VM engine has also been considered.

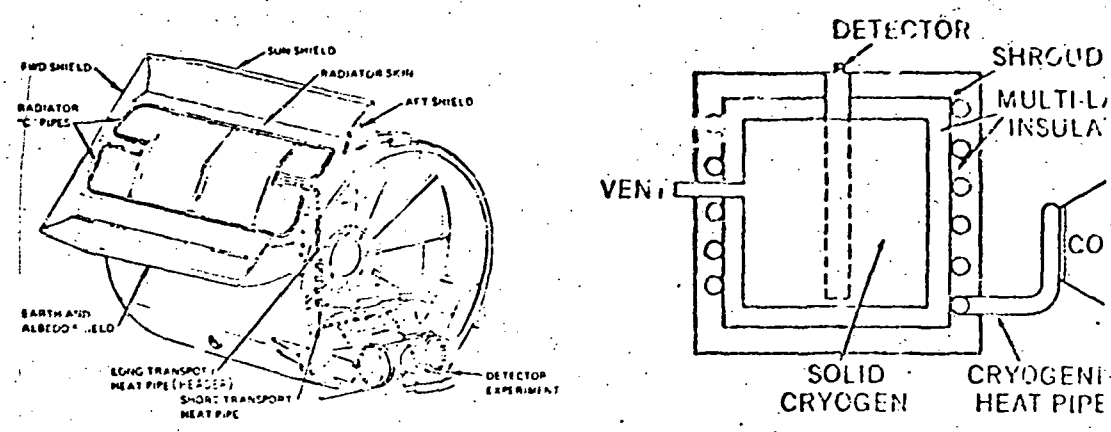

A. Spacecraf and radiator assembly

B. Heat Pipe/Solid Cryogen System

Fig. 2-1 CRYOGENIC HEAT PIPE APPLICATIONS

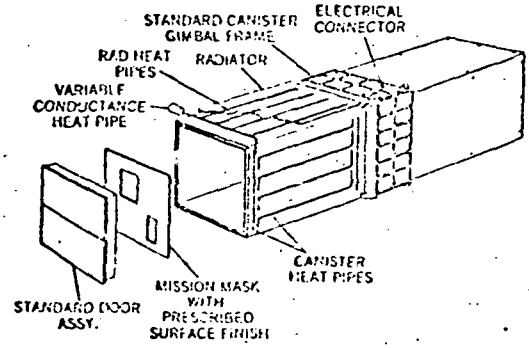

Fig. 2-2 AMBIENT TEMPERATURE
HEAT PIPE APPLICATIONS

Typical requirements for cryogenic heat pipes range from fractions of watts for detector cooling to ten's of watts for large radiant coolers. Corresponding heat transport requirements vary from a few watt-meters to capacities up to 25 watt-meters. Operating temperatures are from 2°K to 250°K depending on the application. High thermal conductances on the order of 1.0 to 10 watt/°C are required since a cryogenic system's efficiency is highly temperature sensitive. The need for variable conductance heat pipes has also been identified with particular emphasis on diodes or thermal switches to protect against hot sink conditions which result from external environmental inputs. Finally, since many of the cryogenic fluids have relatively low wicking heights, wick designs which provide 2-3 times more pumping are desired in order to obtain reliable 1-g performance measurements.

2.1.2 Ambient Temperature Applications

The majority of spacecraft temperature control applications have been near room temperature and considerable experience now exists with axially grooved heat pipes at ambient temperature. Present and future applications include utilization of heat pipes in waste heat rejection, isothermalization and temperature control. In addition to a variety of unmanned spacecraft applications, the advent of the Space Shuttle and Spacelab have created an opportunity to fly a wide variety of scientific instruments which will require relatively low cost temperature control systems. The limited heat rejection services of Shuttle, random orientations due to operational considerations and the variability of requirements with regard to size, geometry, power dissipations and operating temperatures have led to the development of canister concepts utilizing both fixed conductance and variable conductance heat pipes as shown in Fig. 2-2.[e]

Performance requirements for ambient temperature applications range from ten's of watts to multi-hundred watt levels. In the survey conducted under this program, multi-kilowatt requirements for ground applications have

also been identified. Large space systems, such as, the Shuttle primary radiator, also require power dissipations on the order of kilowatts. In most applications, multiple heat pipes are required to collect and distribute the heat. Heat transport requirements for larger systems are in the range of 250 w-m or higher depending on the number of heat pipes used. Operating temperatures fall between 250°K and 325°K. In addition to conventional heat pipes there are also distinct needs for variable conductance technology as illustrated in Fig. 2-2.

2.1.3 Intermediate to High Temperature

Although the bulk of identified heat pipe applications appear to be in the cryogenic to ambient temperature range, intermediate to high temperature requirements also exist. These are derived from radioisotope thermoelectric generators (RTG),[11] solar collectors,[14] and VM engines,[15] etc.

A broad range of performance applies to the intermediate to high temperature range. Isothermalization of RTG radiator fins, for example, poses the need for operation in 350-500°K range. Small, light weight heat pipes (O.D. as small as 0.64-cm (¼-in.)) are desired to accomodate heat loads up to 135 watts with a corresponding transport capability of 70 w-m. Coupling of a heat source with VM engines, on the other hand, will require power levels on the order of kilowatts with transport capacities up to 10,000 w-m depending on the heat source employed (i.e. radioisotope or solar collector). Operating temperatures in the 1000°K range can be expected. Both RTG and VM applications also pose the potential need for gas controlled heat pipe technology.

2.2 Current State-Of-The-Art

For over ten years, axial grooves have been applied to a variety of heat pipe designs including high temperature liquid metal applications. Initially, axially grooved tubing was produced by machining flat stock and forming it into a tube or by broaching a thick wall tube. In aerospace systems, requirements

for lightweight, cost effective designs led to the development of swaged aluminum axially grooved tubing. Subsequently, extruded aluminum grooved tubing was developed which led to better control of the groove form as well as the ability to provide mounting flanges as an integral part of the tubing. Recently, the extrusion process was used to fabricate a closed groove form (Lewis Covert Groove Extrusion), which offers reduced sensitivity to gravity. Recent advances in the state-of-the-art also include the development of a small diameter copper/water axially grooved heat pipe for intermediate temperature application and the extension of axially grooved technology into thermal control applications. Today the status of the technology can be summarized as follows.

2.2.1 Theory

The theory of operation of the axially grooved heat pipe together with mathematical models for hydrodynamic flow is discussed in detail in this report. The Groove Analysis Program (GAP)[16] developed under this contract incorporates current models which account for meniscus recession effects on groove flow properties and fluid inventory; vapor viscous and vapor shear effects; groove geometry effects such as fin tip corner radius; gravity effects; and puddle flow contributions. Either theoretical groove forms or measured groove properties can be used in the program. The model assumes uniform groove properties and liquid distribution, uniform heat input and output, as well as a negligible gravity effect around the circumference of the heat pipe.

Comparisons of predicted values with measured data show good agreement at intermediate operating temperatures and elevations for a number of working fluids. Deviations at extreme conditions are believed to be due to uncertainties in the modeling of vapor effects in the turbulent regime and potential drainage effects on the liquid distribution.

In addition to this computerized model which incorporates a numerical integration solution, a closed form solution was also developed for parametric and design optimization analyses. Incorporated as part of this model is a composite factor (S), which accounts for composite pumping effects and a groove flow factor (N_g) which accounts for meniscus recession effects on liquid flow characteristics. The model is in a dimensionless form which allows evaluation of the heat pipe design independently of size and liquid properties under o-g conditions. Its validity has been verified with GAP predictions and measured data. A complete discussion of the development of this closed form solution and its use is presented in Section 4.0.

2.2.2 Swaged Aluminim Axially Grooved Heat Pipes

Aluminum axially grooved tubing was initially produced for the OAO-B spacecraft[17] with a patented swaging process of the French Tube Division of Noranda Metals, Inc., Newtown, Connecticut. It was fabricated from 6061 aluminum alloy with the groove form shown in Fig. 2-3. Freon 21 was used as the working fluid. The same axially grooved tubing design was used on the OAO-C spacecraft[3] with ammonia as the working fluid. For the ATS-6 spacecraft,[4] a modified design (Fig. 2-4) which yielded improved performance and facilitated tubing fabrication was developed and produced using the same swaging process. Extensive efforts were conducted under the ATS program to develop practical fabrication and processing techniques, and to characterize the performance of the groove design with ammonia. The ATS swaged tubing was also performance tested with nitrogen[18] and methane as working fluids. Measured performance of both the OAO and ATS swaged geometries with various working fluids is summarized in Table 2-1.

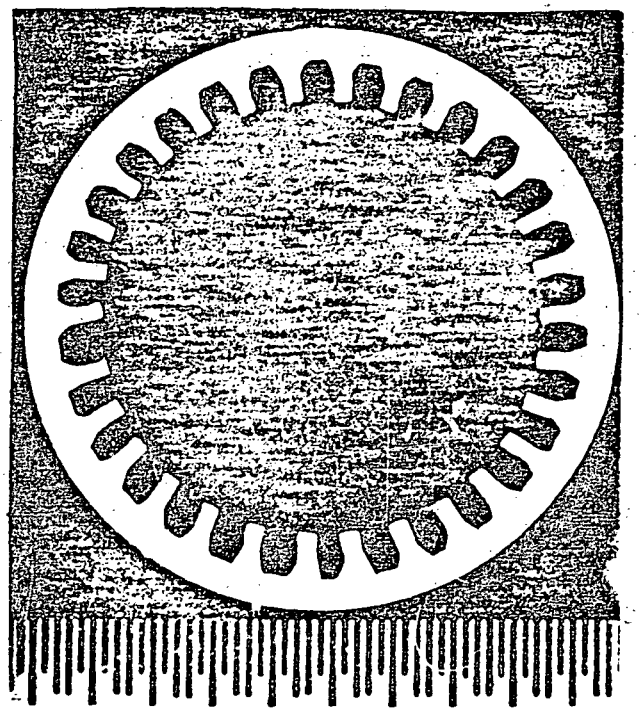

Fig. 2-3. OAO-C Cold-Forged 6061 Aluminum Grooved Tubing

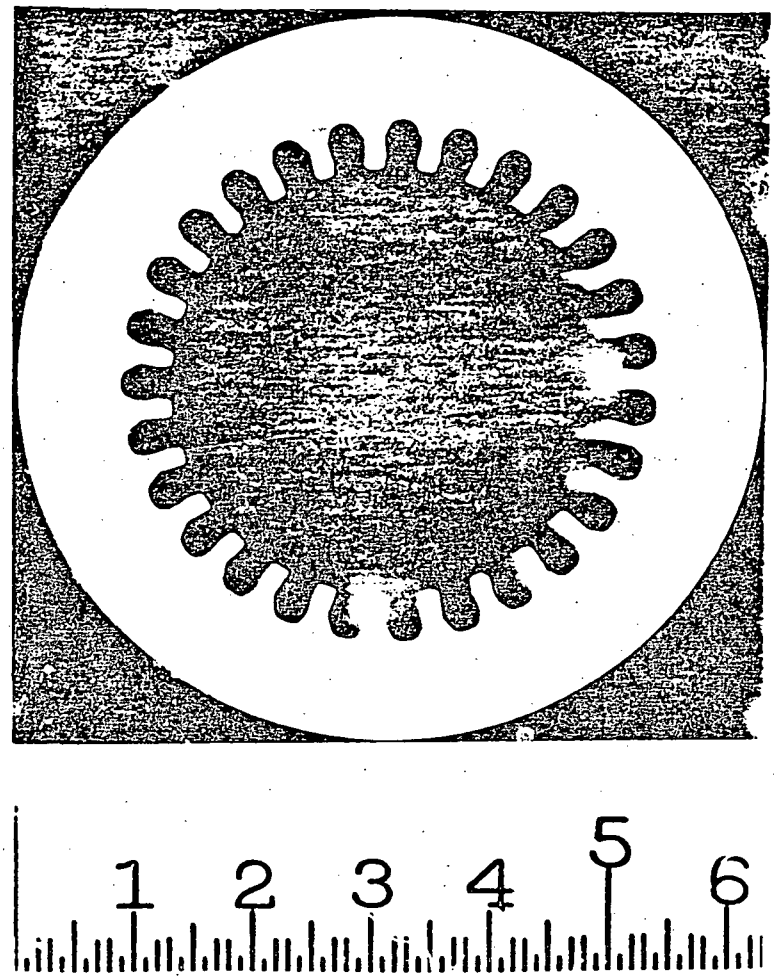

Fig. 2-4. ATS-F Cold-Forged 6061 Aluminum Grooved Tubing

TABLE 2-1. MEASURED PERFORMANCE OF

SWAGED OAO AND ATS AXIALLY GROOVED HEAT PIPES

Fluid	Temp (°K)	o-g Heat Transport Capability (watt-m)	Static Height (cm)	Film Coefficient (w/m^2 - °C) Evaporator	Condenser
OAO - Geometry (Aluminum)					
Ammonia	295	130	1.09	7265	9480
Freon 21	295	28	0.51	1135	1700
Freon 23	295	12	0.46	653	1135
ATS - Geometry (Aluminum)					
Ammonia	310	145	0.89	5676	8515
Methane	150	18	0.52	1362	--
Nitrogen	80	16	0.30	312	1362

Axially grooved tubing is fabricated in the swaging process from predrawn tubing in an annealed or soft condition. The tube is passed over an internal mandrel with the desired size and groove form. As the tube is passed over this mandrel, external hammers, rotating and striking at extremely high frequency, simultaneously reduce the outer diameter and force the material to flow over the internal mandrel to produce the desired groove form. In producing the ATS aluminum axially grooved tubing, a number of problem areas were encountered including variations in concentricity along the length of the tube, variations in groove area and form, and extreme cold working. It should be pointed out, however, that axially grooved tubing for heat pipes was only produced in 6061 alloy with the swaging process. A more ductile material such as 6063 alloy was never tried.

2.2.3 Extruded Aluminum Axially Grooved Heat Pipes

The difficulties encountered with the swaging process led to the development of extruded aluminum axially grooved tubing. The first extrusion was produced by the Battelle Columbus Laboratories.[19] The groove form, however, was inadequate to meet ATS transport requirements, and the extrusion was too bulky and heavy to meet weight limitations. Shortly thereafter, NASA/GSFC initiated an extrusion development program which led to the successful production of the ATS groove form by Micro Extrusions Division of Universal Alloy Corp. of Anaheim, California. The extruded shapes, as shown in Fig. 2-5, were produced in 6063 alloy. Tubing shown in Fig. 2-5B was also produced in 6061 alloy. The ATS extrusion, (also referred to as the NASA/GSFC Extrusion and the Micro Extrusion) has been extensively tested with a number of working fluids[1] and o-g test data has been obtained from GSFC's Heat Pipe Sounding Rocket Experiments.[5,6,20]

The ATS extrusion has also been applied to the I.U.E. spacecraft platform. An ethane pipe which utilizes this extrusion is currently being evaluated as part of

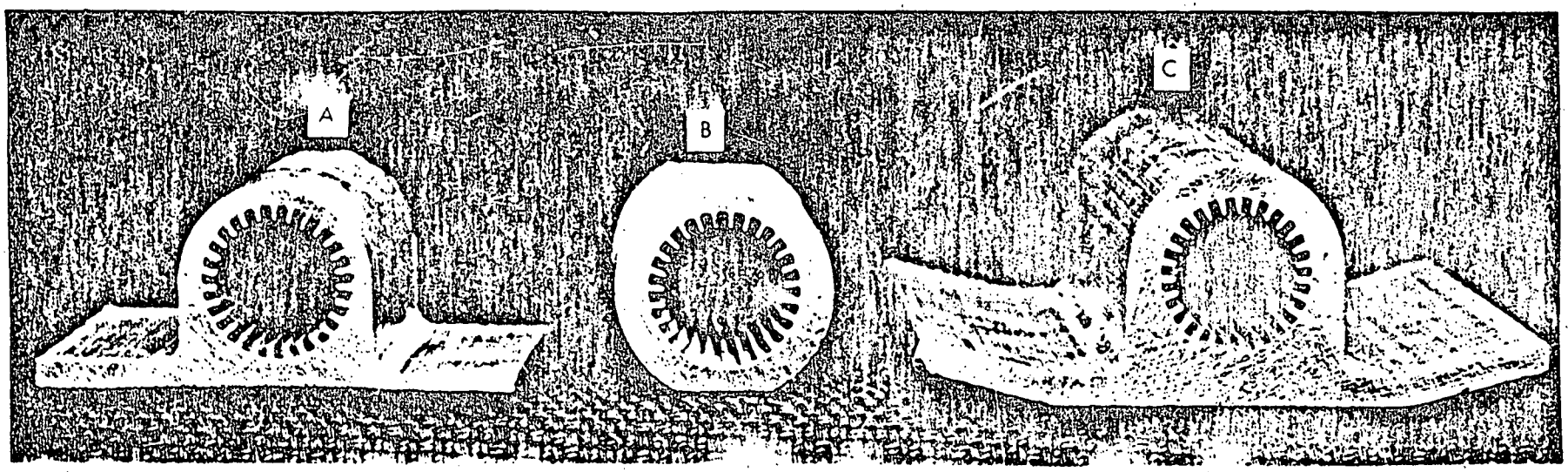

Fig. 2-5. Extruded 6063 Aluminum Grooved Tubing Shapes

TABLE 2-2. MEASURED PERFORMANCE OF

EXTRUDED ATS-6063 AXIALLY GROOVED HEAT PIPES

Fluid	Temp (°K)	o-g Heat Transport Capability (w-m)	Static Height (cm)	Film Coefficient (w/ m^2 - °C) Evaporator	Condenser
Ammonia	203	71.4	2.1	--	--
	223	98.6	2.0	--	--
	250	136	1.9	7000	13600
	273	143	1.6	--	--
Ethane	175	25	1.4	1370	10700
	200	25	1.3	1370	5900
	225	28	1.25	--	--
Methane	100	24.3	1.25	1730	6100
	110	30.4	1.15	1730	6100
	125	33.4	1.1	1730	6100
	140	23.6	1.1	--	--
	155	13.3	1.0	--	--

the Heat Pipe Experiment Package (HEPP)[21] for a potential flight aboard the Long Duration Exposure Facility (LDEF). A summary of available performance data for the ATS extrusion is given in Table 2-2.

Recently, a new groove form designed to reduce the sensitivity to gravity testing has been developed by NASA Lewis.[22] The NASA Lewis Covert Groove extrusion, shown in Fig. 2-6 was produced from 6063 aluminum alloy by Micro Extrusions. Testing was performed with ammonia as the working fluid. Measured performance is summarized in Table 2-3. As can be seen, a substantial improvement in static wicking height has been achieved with the heat pipe fully primed. However, as indicated by the test results, the heat pipe did not reprime at 48% of its static wicking height (12mm) with heat loads greater than 36% (50 watts) of its fully primed capacity at that elevation. This was to be expected since the composite factor (S) (cf. Section 4.4) of the Covert Groove is approximately 1.45. Hence, once deprimed (mechanically or thermally) the static wicking height of this design is approximately 17.2 mm with a 0-g capability of 179 W for a .55 m transport length. Hence, recovery at 12 mm with more than 60 watts is not possible. This, however, does not present a serious problem since the groove form can be modified to minimize the composite factor while retaining the same static wicking height with equal or better performance (cf. Chapter 4.0).

Experience to date indicates that the extrusion process is the best method for producing aluminum axially grooved tubing. Well defined groove forms and good dimensional control have been achieved. Mounting flanges can be extruded as an integral part of the tubing which can simplify interfacing in many applications. In addition, the ability to produce complex groove forms has been demonstrated by the NASA Lewis Covert Groove extrusion which should lead to higher performance and greatly reduced sensitivity to 1-g testing.

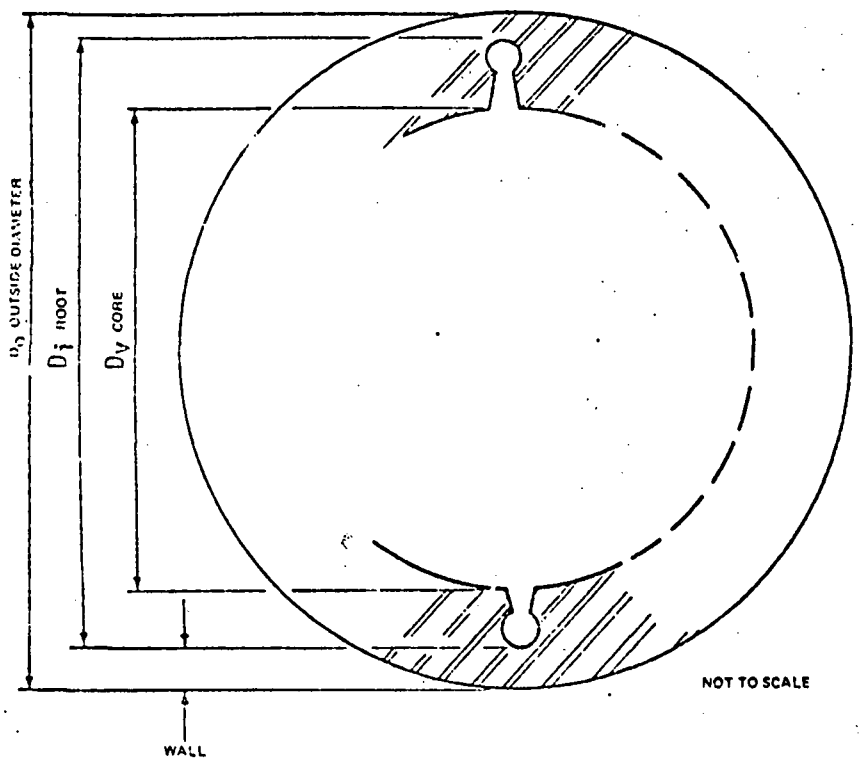

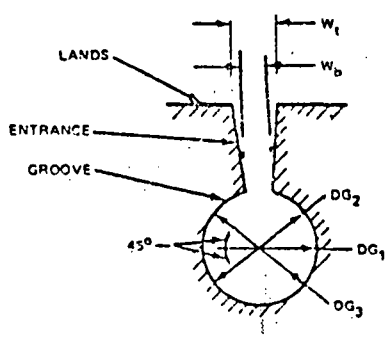

Outer Diameter	D_o = 12.67mm
Root Diameter	D_i = 11.37mm
Core Diameter	D_v = 9.28mm
Entrance Width	W_t = .267mm
Groove Opening	W_b = .218mm
Groove Diameter	DG_1 = .808mm
	DG_2 = .798mm
	DG_3 = .810mm
Wall Thickness	t_w = .640mm
Number of Grooves	N = 20

FIG. 2-6. COVERT GROOVE CHARACTERISTIC DIMENSIONS

TABLE 2-3. PREDICTED PERFORMANCE OF AXIALLY GROOVED HEAT PIPES WITH EXTURDED COVERT GROOVE

Fluid	Temp (°K)	c-g Heat Transport Capability (w-m)	Static Height (cm)	Film Coefficient (w/m² - °C) Evaporator	Condenser
Ammonia	273	160	2.95	--	--
	293	143	2.51	7300	20500
	313	121	2.06	--	--
Methane	100	30	2.71	--	--
	120	34	2.13	--	--
	140	28	1.54	--	--
Ethane	160	27	2.56	--	--
	180	33	2.21	--	--
Propane	233	25	1.95	--	--
	273	21	1.36	--	--
	313	13	0.81	--	--
Butane	273	21	1.78	--	--
	303	19	1.46	--	--

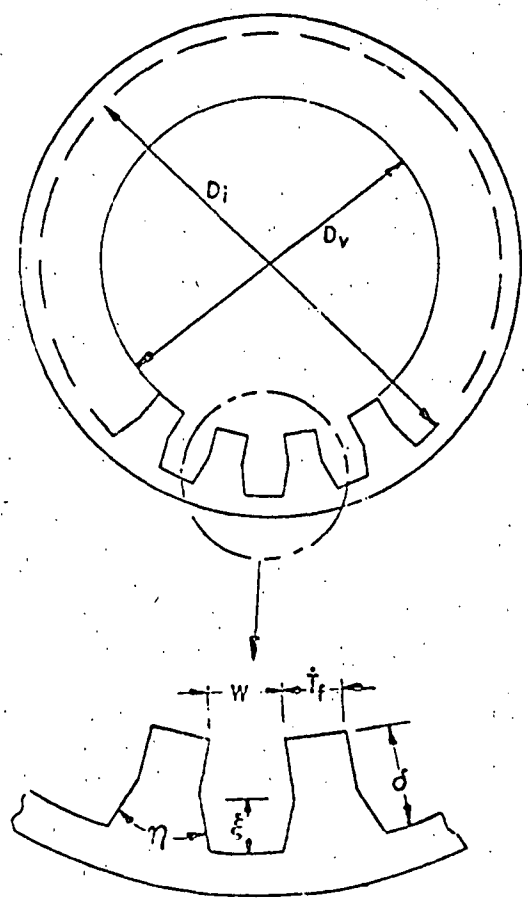

Outer Diameter	D_o = 7.94mm
Root Diameter	D_i = 6.88mm
Core Diameter	D_v = 5.64mm
Groove Width	w = .452mm
Groove Depth	δ = .622mm
Land Thickness	t_f = .432mm
Draft Angle	η = 37 deg.
Draft Depth	ξ = .338mm
Number of Grooves	N = 24

FIG. 2-7. CHARACTERISTICS OF COPPER AXIALLY GROOVED TUBING

2.2.4 Swaged Copper Axially Grooved Heat Pipes

Material properties limit aluminum to a maximum operating temperature of approximately 425°K, where the strength of both 6061 and 6063 alloys begins to fall off rapidly. Also, the best fluid available for the intermediate range is water which is totally incompatible with aluminum. For the intermediate to high temperature range, therefore, axially grooved tubing of materials such as copper and its alloys, stainless steel, carbon steels and super alloys is required, and the swaging process is the only known process which can effectively be used today to produce axially grooved tubing in these materials on a cost effective basis.

During the past year, an extensive effort has been conducted by B & K Engineering and Teledyne Energy Systems to develop a small diameter copper/water axially grooved heat pipe for application to the isothermalization of radiator fins of a radioisotope thermoelectric generator (RTG).[11] An internal surface coating designed to enhance surface wetting developed as part of the effort has demonstrated excellent stability in continuous operation at a temperature of 500°K The geometry of the copper axially grooved heat pipe is shown in Fig. 2-7.

2.2.5 Thermal Control Applications

As indicated earlier, a number of upcoming space missions require the utilization of thermal control heat pipes to maintain temperature stability with varying heat loads and/or sink conditions. Until recently, however, axially grooved heat pipes had been used predominantly in fixed conductance applications. It was only within the past few years that they were used as an ambient temperature gas controlled variable conductance device.[7,8] At cryogenic temperatures, the ATS Extrusion has been tested in various thermal control modes, including active and passive gas controlled variable conductance (VCHP), gas controlled diode,

liquid trap diode and as a thermal switch.[9] A number of ambient temperature gas controlled VCHP designs have been tested by NASA/GSFC for potential application to Shuttle payload thermal control canisters.[10]

Limited published data is available to ascertain axially grooved heat pipe performance in thermal control designs. Unpublished data[23] indicates performance degradation in the gas controlled VCHP's tested by GSFC. The amount of degradation, however, is not consistent with variations occuring mostly among the different vendor designs. Degradation seems to be related to the gas reservoir transition wick interface design, although some degradation in performance has also been noticed when non-condensible gasses were introduced into a fixed conductance pipe using the Lewis Covert Groove Extrusion.[22] It isn't clear at this point whether some degradation is inherent in gas-controlled VCHP applications or whether it is solely gas reservoir design dependent.

In other aspects, the ATS Extrusion has performed as anticipated.[9] Control to within ± 1°C was obtained with feedback control versus ± 10°C with the same system operating in a passive mode. Tests conducted in a liquid trap diode mode indicate that the energy associated with shutdown is approximately twice the latent heat associated with the inventory required to fill the heat pipe (1.6 w-hrs shutdown energy for the configuration tested). The backflow due to heat piping during shutdown is therefore minimal. Operation of a thermal switch was also demonstrated using a liquid trap as a second heat pipe. The simultaneous heat piping action by the liquid trap had a negligible effect on the diode's shutdown.

3.0 ANALYSIS AND DATA CORRELATION

3.1 Introduction

A number of analytical models have been developed over the years to predict axially grooved heat pipe performance. The early models[24,25] used closed form solutions to predict the heat transport capability of rectangular groove cross-sections. Later, computerized solutions of the applicable differential equations were used to predict the thermal conductance[26,27] as well as transport capability.[28] The analytical model developed for the ATS Grooves[28] considered measured groove geometries and for the first time, the effect of meniscus recession and fluid inventory on heat transport performance. While this was a fairly comprehensive treatment of the phenomena associated with undercharge behavior, only a limited effort was devoted to correlating measured data. Furthermore, the model did not account for losses due to liquid/vapor shear interaction and 1-g puddle flow effects.

The liquid/vapor shear term has been demonstrated to be a significant loss factor when operating at high vapor velocities resulting from high heat throughput or low vapor pressures near and below one atmosphere. Excess fluid on the other hand, can create a puddle, which will contribute to the overall heat pipe performance in 1-g, but not, however, in o-g. Excess fluid, which can be a result of either overcharge or drainage from the upper grooves, not only increases the heat transport at low elevations, but can also significantly increase the measured hydrostatic head at high elevations. Both result in an erroneous extrapolation to o-g performance.

A significant portion of the effort conducted under this program, therefore, was directed at the development of a reliable model, incorporating up-to-date theory, and the verification of the model against measured performance data.

The analysis was limited to an evaluation of the hydrodynamic behavior of the axially grooved heat pipe including vapor shear interaction, effect of adverse tilt in 1-g, and puddle flow. Thermal modeling of evaporator/condenser conductances was investigated in a concurrent effort at GSFC.[29,30] The effort conducted under the present program culminated in the development of a comprehensive groove analysis computer program (GAP), which is described in detail in Ref. 16. GAP has been used to predict the performance of the ATS groove form with ammonia, ethane and methane at various operating temperatures, elevations and fluid fills and predictions were compared to measured data. The following section presents a description of the mathematical model and a comparison of predictions with measured data.

3.2 Capillary Pumping Limit

The mathematical model for the capillary pumping limit in the axially grooved heat pipe was developed on the basis of the assumptions illustrated in Fig. 3-1. The heat pipe consists of single evaporator and condenser regions with uniform heat addition and removal separated by an adiabatic section. This model is typical of many applications and is most useful in obtaining standardized performance predictions that can be applied to various conditions. To accomodate multiple evaporators and/or condensers, equivalent QL can be used or actual heat input/output boundary conditions can be incorporated into the model once the points of zero mass transfer have been identified. Similarly non-uniform axial heat load distributions can be specified.

The model is based on independent and uniform grooves equally affected by body forces. It was assumed that no drainage occurs between grooves and that each groove is filled with the same liquid inventory. The assumption of zero-communication between the grooves is based on measured data which indicates that under normal conditions the grooves perform independently of one another.

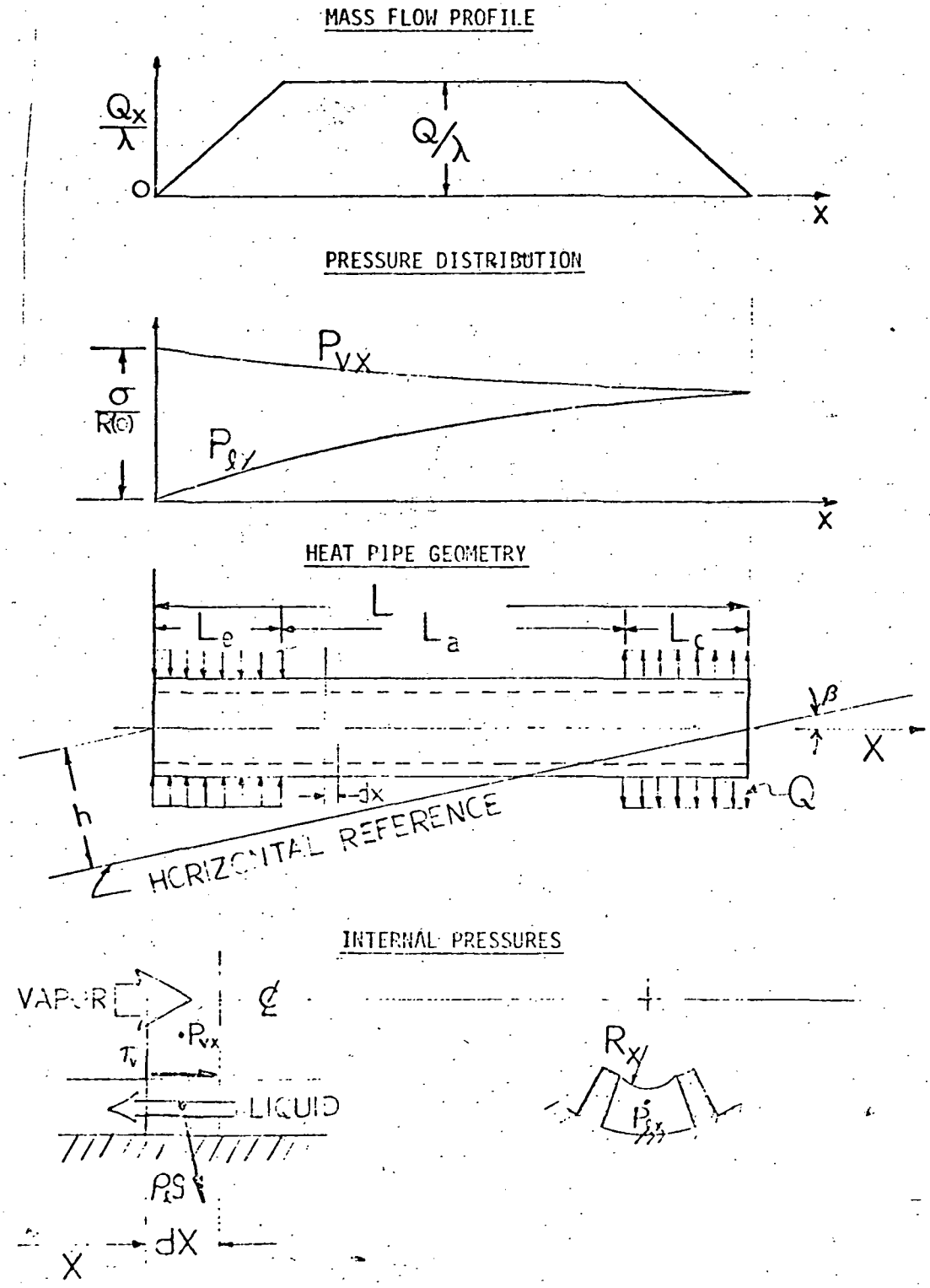

Fig. 3-1. Heat Pipe Flow Conditions

Symmetric heat load conditions were also assumed in the development of the model. Asymmetric heat loads and heat transfer in the wall of the heat pipe as they affect partial burnout, and groove drainage were not considered because of the complexity of combining heat transfer with the hydrodynamics.

The basic formulation of the model with these assumptions is discussed below.

3.2.1 Pressure Balance

Mass flow and pressure profiles corresponding to uniform heat input and output as well as the forces acting within a typical element inside the heat pipe are shown in Fig. 3-1. As heat is added to one end and removed from the other, flow develops within the heat pipe and a pressure differential is developed between the liquid phase and the vapor phase as shown in the pressure profile. This pressure difference is highest at the evaporator and approaches zero at the end of the condenser. For steady-state operation the interfacial pressure difference across the meniscus surface is balanced by capillary forces developed by the groove opening. The pressure balance in any location along the heat pipe can be written as follows:

$$p_{v,x} - p_{\ell,x} = \sigma \left(\frac{1}{R_{1,x}} + \frac{1}{R_{2,x}} \right) \qquad (3\text{-}1)$$

In an axially grooved heat pipe, the two principle radii of curvature at the meniscus interface consist of a finite radius characterized by the groove width and an infinite radius along the groove axis. In the differential form, the axial variation of the interfacial pressures can be written as follows:

$$\frac{dp_{v,x}}{dX} - \frac{dp_{\ell,x}}{dX} = - \frac{\sigma}{R_x^2} \frac{dR_x}{dX} \qquad (3\text{-}2)$$

where R_x is a single principle radius of curvature of finite value at any location X.

3.2.2 Vapor Flow Losses

Vapor flow is dominated by viscous forces. Two types of vapor flow conditions, laminar or turbulent, can exist within the heat pipe depending on the working fluid properties, operating temperature range, and heat flow. In the laminar range where the Reynolds number (Re_v) is the less than 2000 the velocity profile approaches the usual parabolic shape of the Hagon-Poiseuille flow. For this case, the vapor drop is given by:

$$\frac{dp_{v,x}}{dX} = - \frac{32\ \mu_v\ \dot{m}_{v,x}}{\rho_v\ A_v\ D_{hv}^2} \qquad (3\text{-}3)$$

Fluid properties and vapor flow characteristics are assumed constant over the length of the pipe. Meniscus recession has only a second order effect on the vapor space.

At Reynolds numbers above 2000, the vapor flow enters the transition and turbulent range. The Blasius Eq. for turbulence is used to predict the vapor pressure drop in this regime.

$$\frac{dp_v}{dx} = -\frac{0.156\ \mu^2_v}{\rho_v\ D^3_{hv}}\ Re_v^{1.75} \qquad (3\text{-}4)$$

$$\text{where } Re_v = \left[\frac{\rho\ VD}{\mu}\right]_v = \left[\frac{Dm}{A\mu}\right]_v$$

The model is limited in this case since the onset of turbulence is not well defined and also because the axial variation of Reynolds number with the flow changing from laminar to turbulent must also be taken into account. This analysis does not account for the momentum pressure drop and radial vapor flow effects because they are generally small for most spacecraft heat pipe applications.

3.2.3 Liquid Flow Losses

Laminar flow generally prevails in the liquid phase unless pumping is assisted by external forces (e.g. reflux operation). In most wick designs (e.g. screen wicks) the Hagon-Poiseuille equation for laminar flow can be applied directly. However, in axially grooved heat pipes where the channels are uncovered, the shearing effect caused by the counterflow of the vapor against the liquid can induce a significant pressure loss in the liquid flow. Hufschmidt, et. al.[25] determined an empirical experession for a rectangular groove whose depth is greater than the groove width, which accounts for this loss.

In the liquid, pressure gradients resulting from these body forces can either augment or reduce the available capillary pumping. Body forces in a heat pipe are divided into normal and parallel force components as follows:

(a) Parallel force component

$$\left(\frac{dp_{b,x}}{dx}\right)_{\parallel} = \rho_{\ell} g_{\parallel} \tag{3-16}$$

(b) Normal force component

$$\left(\frac{dp_{b,x}}{dx}\right)_{\perp} = \rho_{\ell} g_{\perp} \tag{3-17}$$

In the axially grooved heat pipe, the normal component is usually small compared to the parallel component as long as the grooves are non-communicative and as long as the groove depth is small compared to the static height capability of the groove. In actual static height measurements performed by Molt[31] groove depth effects were determined to be less than 10% for groove aspect ratios $(\frac{\delta}{W})$ greater than one. For the ATS groove form the effect of the groove depth on the top groove's capillary pumping is less than 6%.

In addition the normal component acts on the liquid in the groove in varying degrees depending on circumferential location. It will tend to drive the working fluid out of the top grooves and into the bottom grooves, and the net effect of groove depth on average performance is further reduced. For these reasons, the normal force component was excluded from the analysis and only the parallel component was included in the flow model. For the heat pipe configuration shown in Fig. 3-1, Eq (3-16) for the parallel body force component can

$$V_{\ell x} = \frac{\dot{m}_{\ell x}}{\rho_\ell A_{\ell x}} \tag{3-11}$$

$$\psi = \frac{R_i - R_v}{\mu_\ell} \frac{\rho_\ell A_\ell}{\dot{m}_\ell} \frac{R_v}{2} \left(\frac{dp_{vx}}{dx}\right) \tag{3-12}$$

Using Eqs. (3-3) and (3-6), Eq. (3-12) becomes

For laminar vapor flow ($Re_v < 2000$)

$$\psi = \frac{4 (R_i - R_v)}{R_v} \frac{\nu_v}{\nu_\ell} \frac{A_\ell}{A_v} \tag{3-13}$$

For turbulent vapor flow ($Re_v > 2000$)

$$\psi = 0.0328 \frac{R_i - R_v}{R_v^{0.25}} \frac{A_\ell}{A_v^{1.75}} \frac{\mu_v^{0.25}}{\rho_v \nu_v} \dot{m}_v^{0.75} \tag{3-14}$$

The groove aspect ratio of Eq. (3-6) can be expressed as

$$\phi = \frac{(R_v + R_t) \sin \frac{\pi}{N} - R_t}{R_i - R_v} \tag{3-15}$$

3.2.4 Body Forces

The body forces exerted on the liquid can be derived from gravitational or other accelerational forces such as centrifugal forces induced by spinning. Body forces affect both the liquid and the vapor, however, their effect on the vapor is generally negligible because of the low density of the vapor phase.

In the liquid, pressure gradients resulting from these body forces can either augment or reduce the available capillary pumping. Body forces in a heat pipe are divided into normal and parallel force components as follows:

(a) Parallel force component

$$\left(\frac{dp_{b,x}}{dx}\right)_{\parallel} = \rho_\ell g_{\parallel} \tag{3-16}$$

(b) Normal force component

$$\left(\frac{dp_{b,x}}{dx}\right)_{\perp} = \rho_\ell g_{\perp} \tag{3-17}$$

In the axially grooved heat pipe, the normal component is usually small compared to the parallel component as long as the grooves are non-communicative and as long as the groove depth is small compared to the static height capability of the groove. In actual static height measurements performed by Molt[31] groove depth effects were determined to be less than 10% for groove aspect ratios $(\frac{\delta}{W})$ greater than one. For the ATS groove form the effect of the groove depth on the top groove's capillary pumping is less than 6%.

In addition the normal component acts on the liquid in the groove in varying degrees depending on circumferential location. It will tend to drive the working fluid out of the top grooves and into the bottom grooves, and the net effect of groove depth on average performance is further reduced. For these reasons, the normal force component was excluded from the analysis and only the parallel component was included in the flow model. For the heat pipe configuration shown in Fig. 3-1, Eq (3-16) for the parallel body force component can

be expressed as:

$$\left(\frac{dp_{b,x}}{dx}\right)_{\ell} = \rho_{\ell} g \sin\beta \qquad (3\text{-}18)$$

3.2.5 Capillary Pumping Limit Governing Equations

The liquid and mass flow rates are related to the axial heat flow as:

$$\dot{m}_{\ell,x} = -\dot{m}_{v,x} = -\frac{Q_x}{\lambda} \qquad (3\text{-}19)$$

By combining the preceeding equations for pressure loss and mass flow, and equating them to the capillary and 1-g body force, one obtains the following equations which determine the heat pipe's transport capability within the capillary pumping limit.

For laminar vapor flow ($Re_v < 2000$)

$$\frac{\sigma}{R_x^2}\frac{dR_x}{dx} = \rho_{\ell} g \sin\beta + \left[\frac{8\mu_v}{\rho_v A_v R_v^2} + \frac{\mu_{\ell}}{K_x A_{\ell x} \rho_{\ell}}\left(1 + \frac{\phi^2}{3}\psi\right)\right]\frac{Q_x}{\lambda} \qquad (3\text{-}20)$$

For turbulent vapor flow ($Re_v > 2000$)

$$\frac{\sigma}{R_x^2}\frac{dR_x}{dx} = \rho_{\ell} g \sin\beta + \frac{0.0656\mu_v^{0.25}}{\rho_v A_v^{1.75} R_v^{1.25}}\left(\frac{Q_x}{\lambda}\right)^{1.75} + \frac{\mu_{\ell}}{K_x A_{\ell x}}\left(1 + \frac{\phi^2}{3}\psi\right)\frac{Q_x}{\lambda} \qquad (3\text{-}21)$$

Where ϕ and ψ are defined in Equations (3-15) and (3-13) or (3-14), respectively.

The left hand side of the preceeding equations represents the capillary pumping; the right hand side represents pressure drops as follows:

1. The first term is the hydrostatic loss.
2. The second term is the viscous vapor loss.
3. The third term is the liquid flow loss which combines both the viscous loss and the pressure drop caused by the liquid/vapor shear interaction.

Assumptions made in developing the governing equations are summarized in Table 3-1.

3.2.6 Groove Geometry

A number of basic groove forms, as shown in Fig. 3-2, were considered during the evaluation including:

(a) Trapezoidal Divergent Groove.

This has been the most commonly used groove form in axially grooved heat pipes to date. It has been fabricated in aluminum by cold forging as well as by the hot extrusion process. Recently, a copper groove form has been developed and fabrication of similar groove forms in other materials is currently underway. The main feature of this form is that the two sides diverge. This provides a small groove width in combination with a large liquid flow area.

TABLE 3-1. ASSUMPTIONS FOR CAPILLARY PUMPING LIMIT

GENERAL

1. No drainage and zero-communication between grooves.
2. Steady-state operation.
3. Constant fluid properties for entire system.
4. Symmetric heat addition/removal.
5. No non-condensible gas.
6. Uniform groove properties.

VAPOR FLOW

1. Incompressible flow.
2. Viscous pressure drop is determined by Hagon-Poiseuille Equation for laminar flow; Blasius Equation for turbulent flow.
3. Momentum pressure drop and radial vapor flow losses are negligible.
4. Body force effect is negligible.

LIQUID FLOW

1. Incompressible, laminar flow.
2. Hagon-Poiseuille Equation is utilized for viscous pressure drop.
3. Hufschmidt Equation is applicable for all groove forms to account for vapor shear effect.
4. Negligible gravity effect around the circumference.
5. Only parallel body force is applicable.

FIGURE 3-2. TYPICAL GROOVE GEOMETRIES

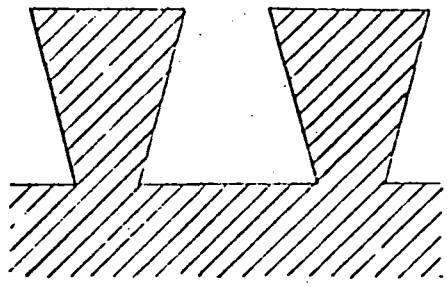

(a) Trapezoidal Divergent

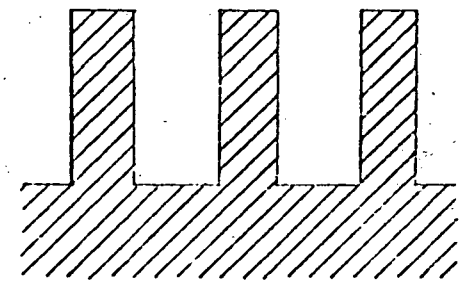

(b) Rectangular

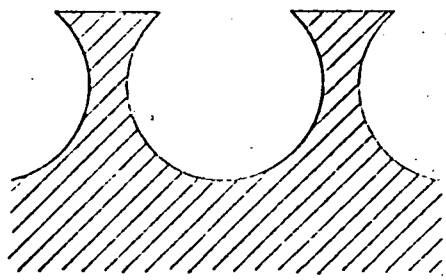

(c) Circular Divergent

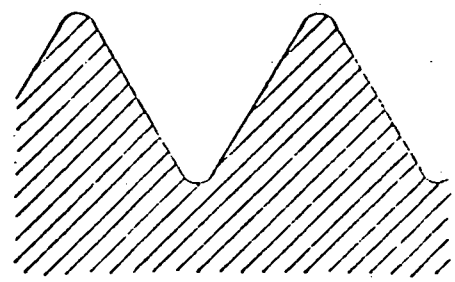

(d) Convergent

(b) Rectangular Groove

This groove form represents a limiting case of the trapezoidal groove in that the two sides of the groove are parallel.

(c) Circular Divergent Groove

This groove form is similar to the trapezoidal form in that it provides a small groove opening in combination with a large flow area. Prototypes of this groove form have been fabricated in aluminum extrusions.

(d) Convergent Groove

This groove form is the opposite of the divergent form. Its minimum pumping radius occurs at the bottom of the groove. The convergent grooves are triangular in shape; they are usually formed in the heat pipe wall by threading and are normally used in combination with slab wicks, spiral arteries, etc. to provide circumferential distribution of the liquid.

For axially grooved heat pipe applications, low liquid flow impedance in combination with high pumping is desired. Only divergent grooves, therefore, were considered in detail. The basic forms and geometrical properties of the trapezoidal divergent and circular divergent are summarized in Figures 3-3 and 3-4, respectively.

3.2.7 Solutions of the Governing Equations

The governing equations (3-20) and (3-21) are best solved by numerical methods. A computer program (GAP) as described in Section 3.5

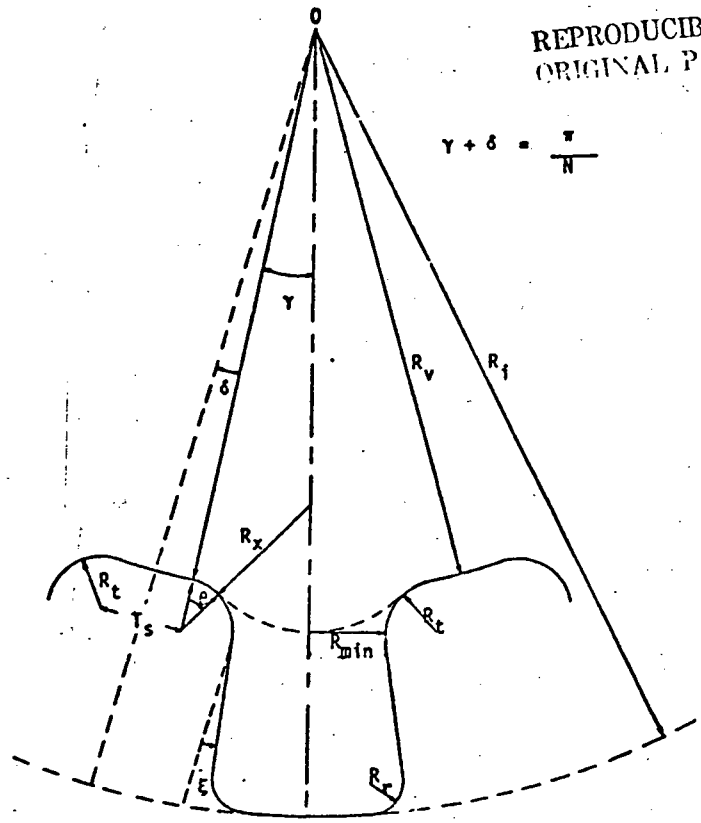

FIGURE 3-3. TRAPEZOIDAL GROOVE PROPERTIE

Liquid Flow Area

$$A_{\ell x} = N\Big\{\gamma R_i^2 - (R_v + R_t)(R_x + R_t)\sin\theta - R_t^2(\delta + \tfrac{\pi}{2} - \theta) - 2(R_i - R_v - R_t)R_t - 2R_r^2(1 - \tfrac{\pi}{4}) + \delta(R_i - R_v - R_t)^2 - (R_i - R_v - R_t + \tfrac{1}{2}R_t\xi)^2\xi - R_x^2(\gamma + \theta)\Big\}$$

Wetted Perimeter

$$WP_x = N\Big\{2(\delta + \theta)R_i - T_s - 2R_t - 2R_r + \pi R_r + 2(\delta + \tfrac{\pi}{2} - \theta)R_t + 2(R_i - R_v - R_t) - 2(R_i - R_v - R_t)\xi\Big\}$$

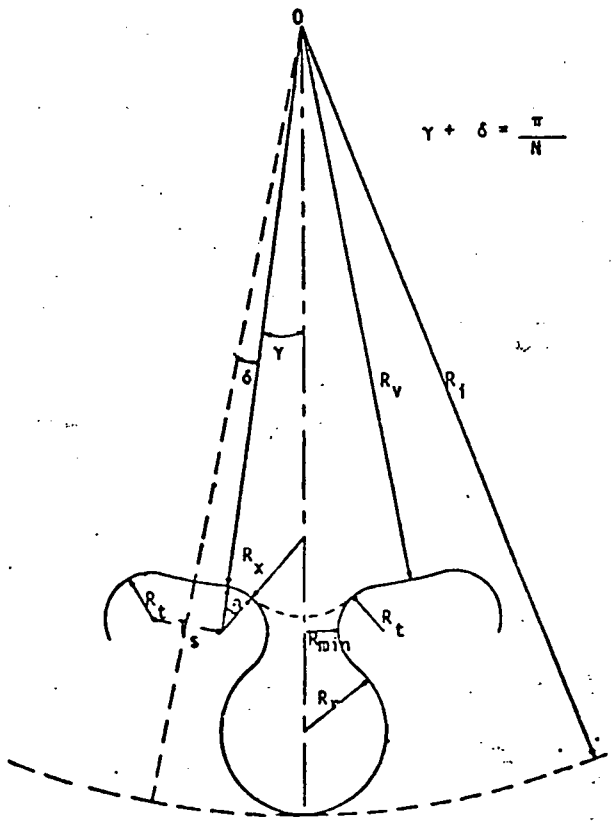

FIGURE 3-4. CIRCULAR CONVERGENT GROOVE GE

Liquid Flow Area

$$A_{\ell x} = N\Big\{(R_v + R_t)(R_i - R_r)\sin\gamma - (R_r + R_t)(R_x + R_t)\sin\theta - (\xi - \theta)R_t^2 + (\xi - \gamma)R_r^2 - R_x^2(\theta + \gamma)\Big\}$$

Wetted Perimeter

$$WP_x = 2N\Big\{R_t(\xi - \theta) + R_r(\xi + \gamma)\Big\}$$

was developed for this purpose. The computer program uses the fourth order Runge-Kutta integration method with self-adjusting step sizes. Specified inputs required to solve the governing equations include working fluid properties, groove geometries as defined in Section 3.2.6, heat pipe diameter and number of grooves. In addition initial conditions and heat distribution are also required to completely specify the problem. Referring to Fig. 3-1, the axial heat flow rate Q_x can be expressed in terms of total heat input Q for each of the heat pipe regions. For uniform heat input in a single evaporator/single condenser heat pipe separated by an adiabatic section, Q_x can be expressed as follows:

$$\begin{aligned} &\text{Evaporator:} && 0 < X < L_e && , && Q_x = \frac{QX}{L_e} \\ &\text{Adiabatic:} && L_e < X < L_e + L_a && , && Q_x = Q \\ &\text{Condenser:} && L-L_c < X < L && , && Q_x = \frac{Q(L-X)}{L_c} \end{aligned} \qquad (3\text{-}22)$$

Equations (3-20) and (3-21) are solved numerically by specifying an initial value of Q and a minimum radius of curvature equal to half the groove width at the end of the evaporator. The local radius required to support the fluid flow is then determined at each axial location by integrating from the evaporator to the condenser end. Once the radius of curvature is known the corresponding fluid inventory is readily obtained. If the resulting meniscus radius at the end of the condenser is less than one half the vapor diameter, the calculations are repeated by increasing the heat load until the maximum heat load is reached. The maximum heat load is achieved when the

meniscus at the condenser end is equal to ½ D_v. The above calculations can be repeated for various elevations until a family of curves of Q versus charge and elevation are obtained.

3.3 Other Heat Flow Limits

In addition to the capillary pumping limit, sonic and entrainment limits are also evaluated by the GAP program.

3.3.1 Sonic Limit

The vapor velocity in the heat pipe evaporator increases steadily along its length and reaches a maximum at the evaporator exit. The maximum vapor flow which can exist there is the sonic velocity. The axial flow corresponding to the sonic limit is therefore (Ref. 32).

$$Q_s = (\rho A)_v \lambda \sqrt{\frac{\gamma R_o T}{2 (\gamma + 1) M}} \qquad (3\text{-}23)$$

3.3.2 Entrainment Limit

The entrainment limit is also associated with high axial vapor flow velocities. Since liquid and vapor are in direct contact along the heat pipe, a shear force exists at their interface. At low relative velocities the shear force merely increases the viscous drag for both phases. As the relative velocity becomes greater the interface becomes unstable, and small liquid droplets are torn from the liquid surface and entrained into the vapor. This entrainment phenomenon reduces the amount of liquid pumped back to the evaporator and the heat transport capability is reduced.

Entrainment is associated with the Weber number which is a ratio of inertial forces in the vapor and tension forces at the liquid surface. A Weber number of unity is generally considered as the onset of entrain-

ment. The corresponding heat transport limit is given by (Ref. 32).

$$Q_e = \sqrt{\frac{\sigma \rho_v}{W}} \lambda A_v \qquad (3\text{-}24)$$

3.4 Excess Fluid Evaluation

The preceding sections dealt with fundamental flow conditions within an axially grooved heat pipe. The model for the capillary pumping limit assumed either completely saturated grooves or partially filled grooves. In actual application, however, the heat pipe is most likely to be slightly overcharged in order to assure a fully saturated condition and, hence, optimum performance. The effect of excess liquid inventory on performance in both o-g and 1-g, therefore, is of interest in the overall evaluation of heat pipe performance.

3.4.1 Zero-G Slug Formation

It is presently theorized that a heat pipe operating in o-g with an overcharge will develop a slug at the downstream end of the condenser. The principal effect of such a liquid slug will be a partial blockage of the condenser section, resulting in a degraded condenser conductance. The larger the quantity of excess liquid, the larger the degradation in conductance. The degree of condenser blockage is dependent on the vapor core cross-sectional area and the shape of the excess slug at the vapor/liquid interface. Unfortunately, little is known about the liquid slug behavior in o-g and no data is available to develop empirical models. Current hypotheses range from deep parabolic shapes maintained by vapor dynamics and extending over significant portions of the condenser to nearly flat interfaces which assume pressure equilibrium with a nearby flat meniscus in the grooves.

Since little condensation will occur directly into the liquid slug, no significant mass flow will occur between the slug and the grooves. A zero liquid mass flow condition and zero vapor flow velocity at the liquid slug interface imply that no pressure gradient exists between the slug and the nearby grooves. Since the meniscus in the nearby grooves consists of only one finite radius of curvature on the order of 0.5 D_v, and since the slug has two finite radii of curvature, the slug must assume a flatter shape than the groove to maintain the neraly zero pressure differential. Assuming a uniform slug with a nearly flat interface its length is:

$$L_{sl} \approx \frac{\Delta m}{\rho_\ell A_v} \qquad (3\text{-}25)$$

where Δm is the excess liquid charge.

3.4.2 Excess Liquid 1-g Puddle Flow

The effect of excess liquid on performance in 1-g can be more signigicant than in o-g. If the overcharge is substantial a puddle will form and heat transport in excess of that furnished by capillary pumping will be realized.

When an axially grooved heat pipe is operated with excess working fluid in 1-g, a puddle will form. There are three distinct liquid flow regions in the heat pipe when there is a puddle. As shown in Fig. 3-5 they are:

(a) Flow in grooves unaffected by the puddle: These grooves extend the full length of the heat pipe. Pumping is derived from capillary forces and equations (3-20) and (3-21) apply for the entire groove provided that the adverse heat pipe

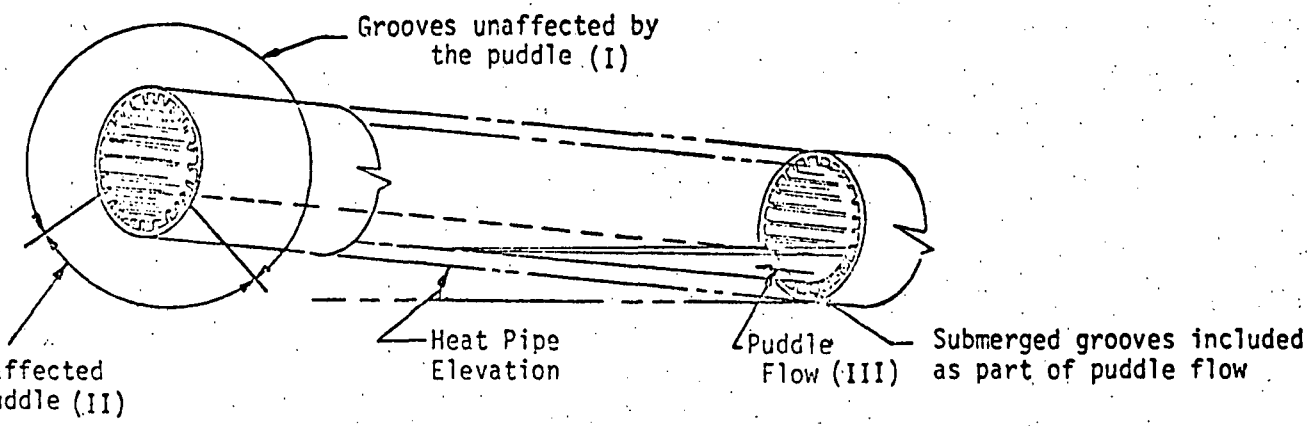

FIGURE 3-5 PUDDLE FLOW SCHEMATIC

elevation is smaller than the theoretical static height. When the heat pipe elevation is greater, the grooves will partially drain, further contributing to the puddle flow. In this case the capillary pumping will be exerted on the groove length where the liquid remains in the grooves.

(b) Flow in the grooves affected by the puddle: For the portion of the grooves extending beyond the puddle, the same pumping behavior as described in the preceding region will occur. In addition, the effect of the puddle on these grooves is a reduction in both their transport length and the actual elevation.

(c) Puddle Flow: Gravity will provide the driving force for the liquid return in the puddle. Pumping along the puddle is provided by the variation in the elevation of the free surface of the puddle.

The presence of a puddle in the heat pipe will affect performance in two ways. It increases the axial liquid return therein increasing heat transport performance, and decreases the pumping elevation to partially submerged grooves. Both effects result in an increase in measured performance. A model designed to predict puddle flow effects in an axially grooved heat pipe was developed and incorporated as part of the GAP program. The puddle flow model considers internal flow and static conditions up to the static wicking height of the unsubmerged grooves. Drainage effects above the static height limit were not included as part of the model. A detailed

derivation of the equations governing puddle flow is presented in Appendix A. The approach taken as well as the resulting equations are presented below.

The model for puddle flow is based on the following assumptions:

(a) Condensation and evaporation are uniform in the axial direction.

(b) The effect of asymmetric heat transfer is neglected.

(c) Flow in the puddle is one dimensional and the Hagon-Poiseuille Equation is applicable to the liquid pressure drop in the puddle.

(d) The interface between the puddle and the groove is continuous without interruption by the groove land (i.e. the land is neglected at the interface).

(e) For the region of the groove extending beyond the puddle, the groove's maximum performance can be predicted by a closed form solution which is proportional to the apparent static height of the portion of the groove unaffected by the puddle and the inverse of its effective length, i.e.

$$Q_g = \frac{(QL)_{max}}{L_{eff}} \left\{ 1 - \beta \frac{L}{h_{max}} \right\} \qquad (3\text{-}26)$$

where the transport capability of a groove $(QL)_{max}$ and the static height (h_{max}) are calculated for a nominal charge by solution of Eqs. (3-20) or (3-21) as discussed previously.

The puddle flow analysis consists of satisfying the Equation of Motion for the puddle and Mass Continuity at the intersection of the puddle and the submerged grooves. The analysis was conducted for the flow model of Fig. 3-6. The governing equations for the puddle in an axially grooved heat pipe are as follows:

Equation of Motion in Puddle

$$\rho_\ell g \cos\beta \frac{R_v}{2} \sin\frac{\theta_p}{2} \frac{d\theta_p}{dX} = \rho_\ell g \sin\beta + \frac{\mu_\ell Q_p(x)}{\lambda(KA)_p \rho_\ell} \quad (3\text{-}27)$$

Eq. (3-27) represents the pressure balance required to satisfy the flow condition. The pumping force is derived from the gravity acting on the free surface of the puddle as shown in Fig. 3-6. This pumping force is denoted by the term on the left hand side of the Eq. (3-27). The hydrostatic and dynamic losses within the puddle are on the right hand side of Eq. (3-27). The first term is the hydrostatic head developed as a result of the pipe inclination. The second term is the liquid viscous loss. Mass flow continuity must exist at the puddle/groove interface and the following equations apply.

Continuity Equation (Mass Flow Continuity)

$$\frac{dQ_p}{dx} = \frac{(QL)_{max}}{2\pi X_{eff}} \left(1 - \beta \frac{X}{h_{max}}\right) \Omega_r \frac{d\theta_p}{dx} + Q_{sp}\Omega_\ell \quad (3\text{-}28)$$

where X_{eff}, Ω_r and Ω_ℓ are shown in Table 3-2. The heat capacity, Q_{sp}, transported by the grooves that are affected by the puddle is:

$$Q_{sp} = \int_0^{\theta} \frac{(QL)_{max}}{2\pi X_{eff}} \left(1 - \beta \frac{X}{h_{max}}\right) d\theta_p \quad (3\text{-}29)$$

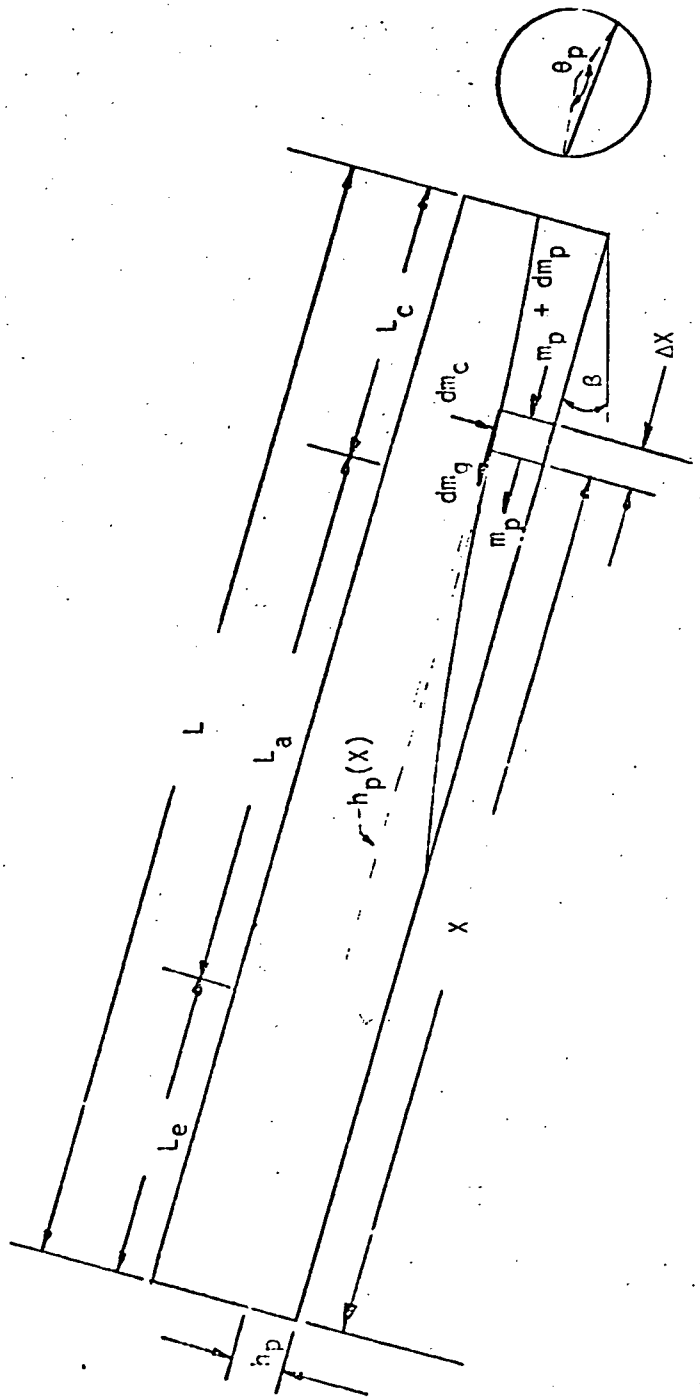

Fig. 3-6. Geometric Parameters of Puddle Flow.

TABLE 3-2. DEFINITION OF FUNCTIONS IN THE GOVERNING EQUATIONS OF PUDDLE FLOW

In the evaporator, $L_e \geq X \geq 0$

$$X_{eff} = \frac{1}{2} X$$

$$\Omega_r = \frac{X}{L_e}$$

$$\Omega_\ell = \frac{1}{L_e}$$

In the adiabatic section, $L_e + L_a \geq X \geq L_e$

$$X_{eff} = X - \frac{1}{2} L_e$$

$$\Omega_r = 1$$

$$\Omega_\ell = 0$$

In the condenser, $L \geq X \geq L_e + L_a$

$$X_{eff} = (X - L_e - L_a)\left[1 - \frac{1}{2L_c}(X - X_a - L_e)\right] + L_a + \frac{1}{2} L_e$$

$$\Omega_r = 1 - \frac{1}{L_c}(X - L_e - L_a)$$

$$\Omega_\ell = -\frac{1}{L_c}$$

The first term of Eq. (3-28) represents the net flow increment across the puddle element. The first term on the right hand side of Eq. (3-28) denotes the flow interchange from the puddle to the groove intersecting the puddle element. The second term is the mass transfer to the free surface of the puddle element.

Eqs. (3-27), (3-28), and (3-29) are solved by the fourth order Runge-Kutta integration method to yeild Q_{sp} and θ_p. Specified conditions required for the solution consist of:

(1) Groove geometry and heat pipe tilt.

(2) Evaporator, transport and condenser lengths.

(3) The starting location of the puddle in the heat pipe.

The total heat pipe transport is calculated by summing the heat capacity Q_{sp} with the heat load carried by the remaining grooves. The fluid inventory is also calculated directly once the puddle angle (θ_p) has been established. Solutions are then obtained for different puddle lengths until the fluid inventory exceeds the specified overcharge. The results can then be interpolated to establish the performance at specified overcharge conditions.

3.5 Groove Analysis Program

The Groove Analysis Program (GAP) was developed to predict the performance of various groove geometries for undercharge and/or overcharge conditions. The program is described in detail in the User's Manual.[16] Both 1-g and o-g conditions are included as part of the program. The code will perform the transport prediction for various heat pipe elevations at the user's option. The following are the principal features of the program:

3.5.1 Capillary Pumping Limit

The capillary pumping limit is obtained by solving the governing Eqs. (3-20) or (3-21) using the fourth order Runge-Kutta method for specified initial conditions, working fluid properties, and axial groove and heat pipe geometries. The axial groove liquid flow characteristics which consist of meniscus radius, permeability, groove area and capillary pumping force are presented in the program output. The groove capillary flow characteristic ($\frac{2\overline{KA}_\ell}{w}$) as well as the gravity, liquid, vapor and liquid/vapor shear losses are also determined and can be utilized in the derivation of an empirical closed-form solution for heat pipes in the groove design optimization study. The GAP normally prints out the above results for the ideal charge condition, however, the transport capability as a function of undercharge will be calculated at the user's option.

3.5.2 Additional Heat Flow Limits

The GAP program will also predict the axial heat flows corresponding to the sonic and entrainment limits. The sonic condition and entrainment usually result during operation at low vapor pressures. Once either limit is encountered in the heat pipe prior to the capillary pumping limit, the program will compute the axial groove flow characteristics on the basis of the sonic or entrainment limit whichever is the smallest.

3.5.3 Geometry and Heat Load Condition

The code is currently able to analyze the following groove forms: trapezoidal, rectangular, convergent (triangular) and circular, which are shown in Fig. 3-2. The analysis is limited to uniform heat addition and removal with single evaporator and condenser sections. The code is programmed in a manner to be easily modified by the user to handle non-uniform heat addition and removal. Multiple and asymmetric heat loading, preferentially filled grooves and drainage are not considered.

3.5.4 Overcharge Condition

A heat pipe operating in o-g with an overcharge will develop a uniform slug at the downstream end of the condenser. The program predicts the o-g slug based on a 1% overcharge relative to the nominal fluid inventory calculated by the program. When the heat pipe is operated with excess working fluid in 1-g, a puddle will form. The program determines total performance, including puddle flow contribution. The program is valid for elevations less than the theoretical static height of the groove. Drainage effects are not included as part of the analysis.

3.5.5 Pressure Containment

The GAP Program also calculates the pressure containment requirements for a heat pipe experiencing temperatures above the critical point of the working fluid. The containment evaluation includes internal pressure of the heat pipe at maximum service temperature and the reservoir volume required to accommodate the maximum allowable pressure determined from the strength of the heat pipe wall material. The internal pressure at the specified service temperature is calculated using the Beattie-Bridgeman Equation of State.

3.6 Predictions and Data Evaluation

The GAP was utilized to predict the heat pipe performance for the ATS-6063 extruded groove tubing with the following working fluids and temperature ranges:

Methane	100 - 150°K
Ethane	150 - 220°K
Ammonia	200 - 300°K

The cross-section of the ATS extruded groove geometry is presented in Fig. 3-7 with the measured groove properties of actual tubing.

ATS Groove Properties

Number of grooves	N	=	27
Vapor Core Diameter	D_v	=	0.864cm
Groove Width	W	=	0.067cm
Groove Depth	δ	=	0.108cm
Groove Root Diameter	D_i	=	1.08cm
Land Thickness	T	=	0.0376cm
Groove Land Taper Angle	ξ	=	3.749 deg
Single Groove Area	A_ℓ	=	$7.704 \times 10^{-3} cm^2$

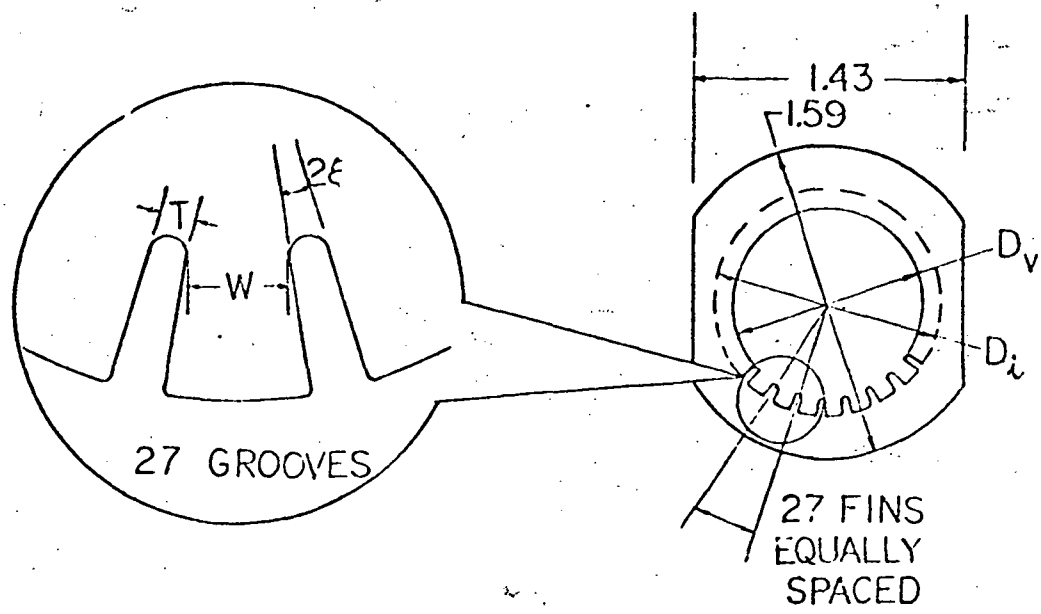

Fig. 3-7. ATS Extruded Geometry.

3.6.1 Data Correlation

Comparisons between predictions and test data[1] are given in Figs. 3-8 through 3-19. The objective of the evaluation was to compare parametric performance data for the various fluids at different operating temperatures with results from the analytical model developed under this study. Discrepancies between measured and predicted performance were evaluated. Generally, the following were noted:

a. At low elevations, the predicted performance is higher than measured data. The lower the temperature the higher this discrepancy. This effect seems to be related to vapor losses and is especially apparent in the turbulent vapor flow regime.

b. At intermediate elevations, good agreement with measured data was obtained.

c. At higher elevations, measured data is substantially higher than predicted. Drainage effects are believed to be causing this difference.

Results obtained for each fluid evaluated are summarized below:

a. Methane

Performance predictions for methane compared to test data from Ref. 1 are shown in Figs. 3-8 through 3-12. The turbulent region is also indicated. As expected, the performance curves become nonlinear in this region. The predicted results indicate that the nonlinear effect of turbulent flow is most pronounced at the lower end of the temperature range. At 100°K there is about a 5 watt discrepancy at the lower elevation (0.254 cm) and the difference decreases as the elevation increases. Near the theoretical static height 1.05 cm, the predicted performance becomes less than the measured values. At 110 and 125°K good agreement is obtained except for the cases

near the theoretical static height. It should be noted that an additional 0.7 g over 7.4 g contributes about 2-5 watts in performance. Above 140°K the deviation from the measured data is significant for those points whose elevations are greater than the theoretical static height. This deviation may be explained by the drainage effect and the drainage evaluation will be presented in the forthcoming section.

b. Ethane

Predicted performance and measured data are presented in Figs. 3-13 through 3-15 for ethane at operating temperatures of 175, 200, and 225°K with 9.3 and 9.8 g charges. The turbulent region is also shown in these Figs. The effect of turbulent flow does not appear significant for the temperature and elevation ranges considered. As in the case of methane, the predicted performance is generally higher than the measured values at lower elevations and lower at elevations near or above the theoretical static height.

c. Ammonia

Performance with ammonia is compared in Figs. 3-16 through 3-19 at temperatures between 200 and 300°K. It should be noted that the evaporator section in these cases is 30.5 cm. At 203°K the vapor flow is laminar throughout all elevations. The theory predicts lower performance if the mean values of the measured data are used for comparisons.

For the temperatures of 223 and 248°K and low elevations, there is a substantial decrease in predicted performance due to the turbulent effect. Turbulence is due to the increased heat transport capacity resulting from improved liquid properties. At very low elevations no data is available for comparison. Near and above the static height, the theory underpredicts

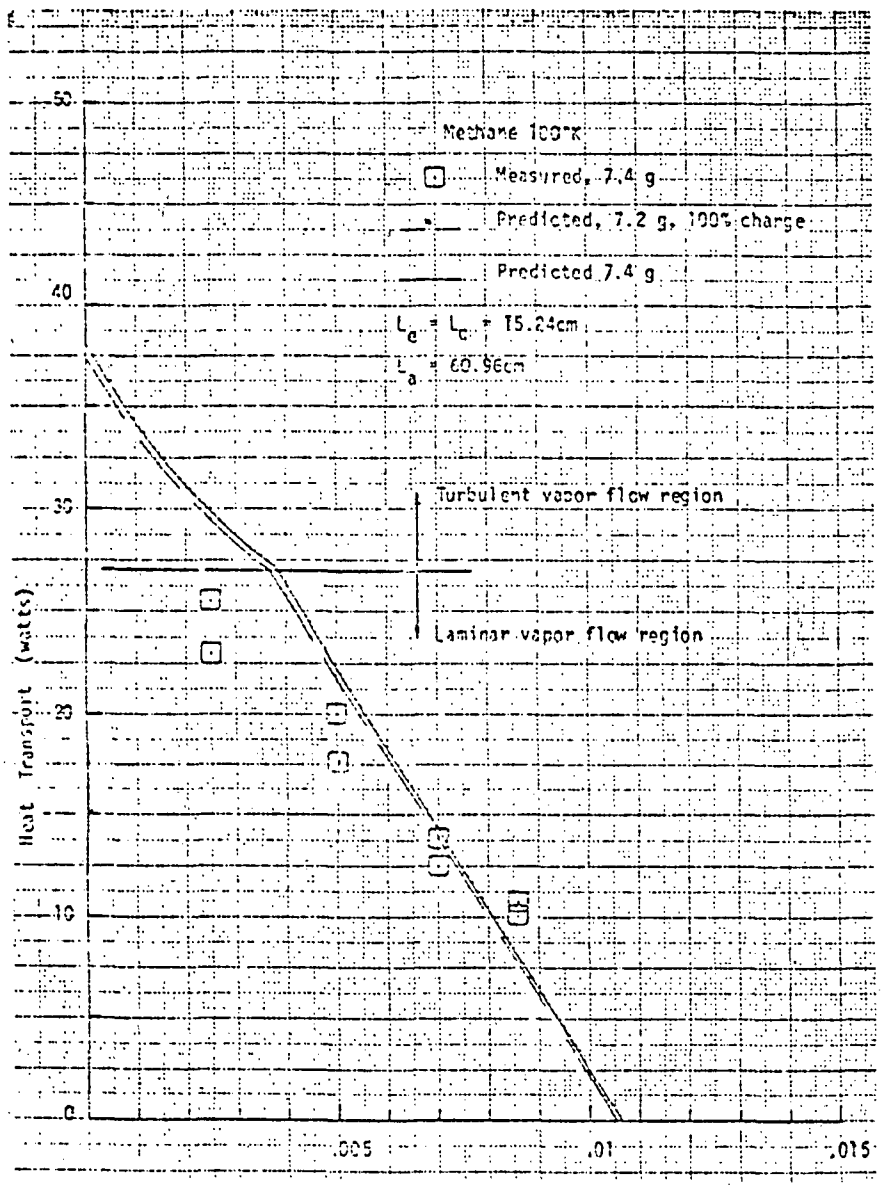

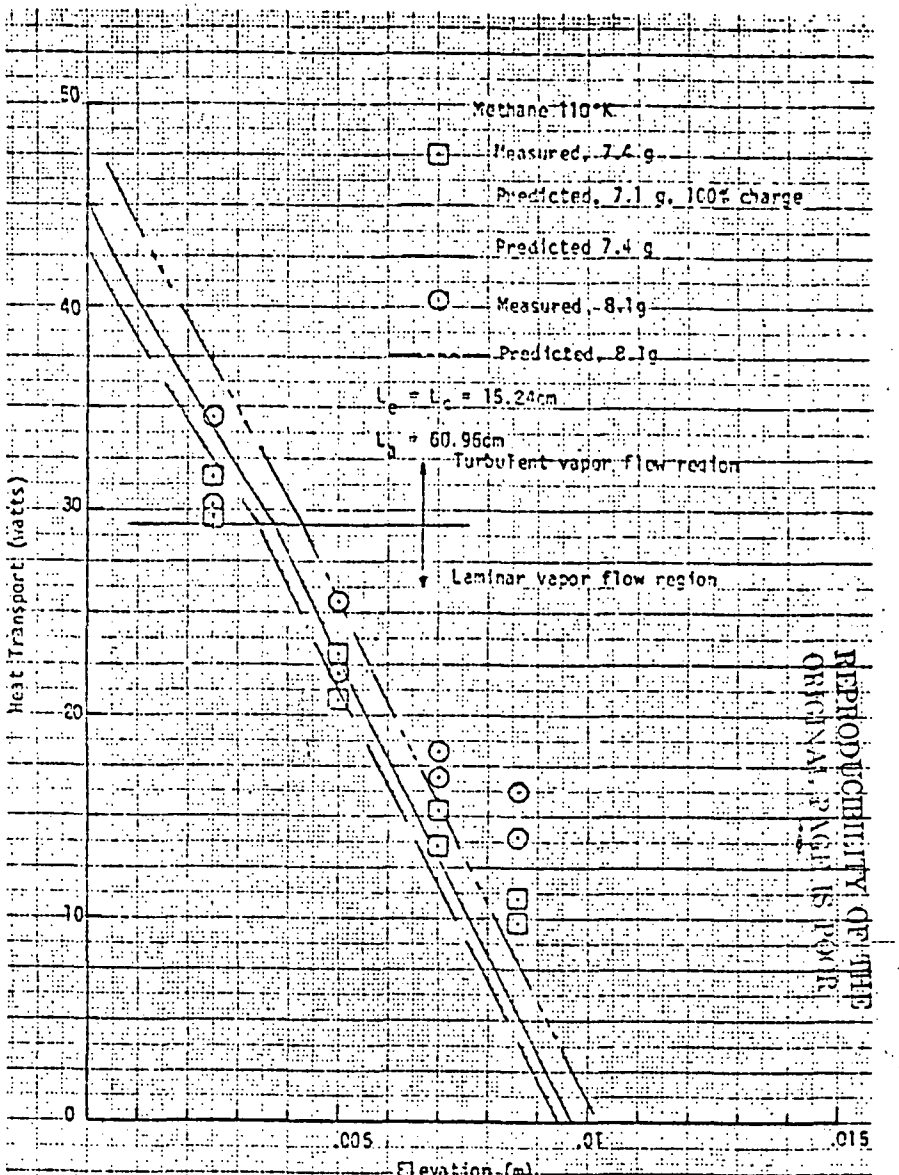

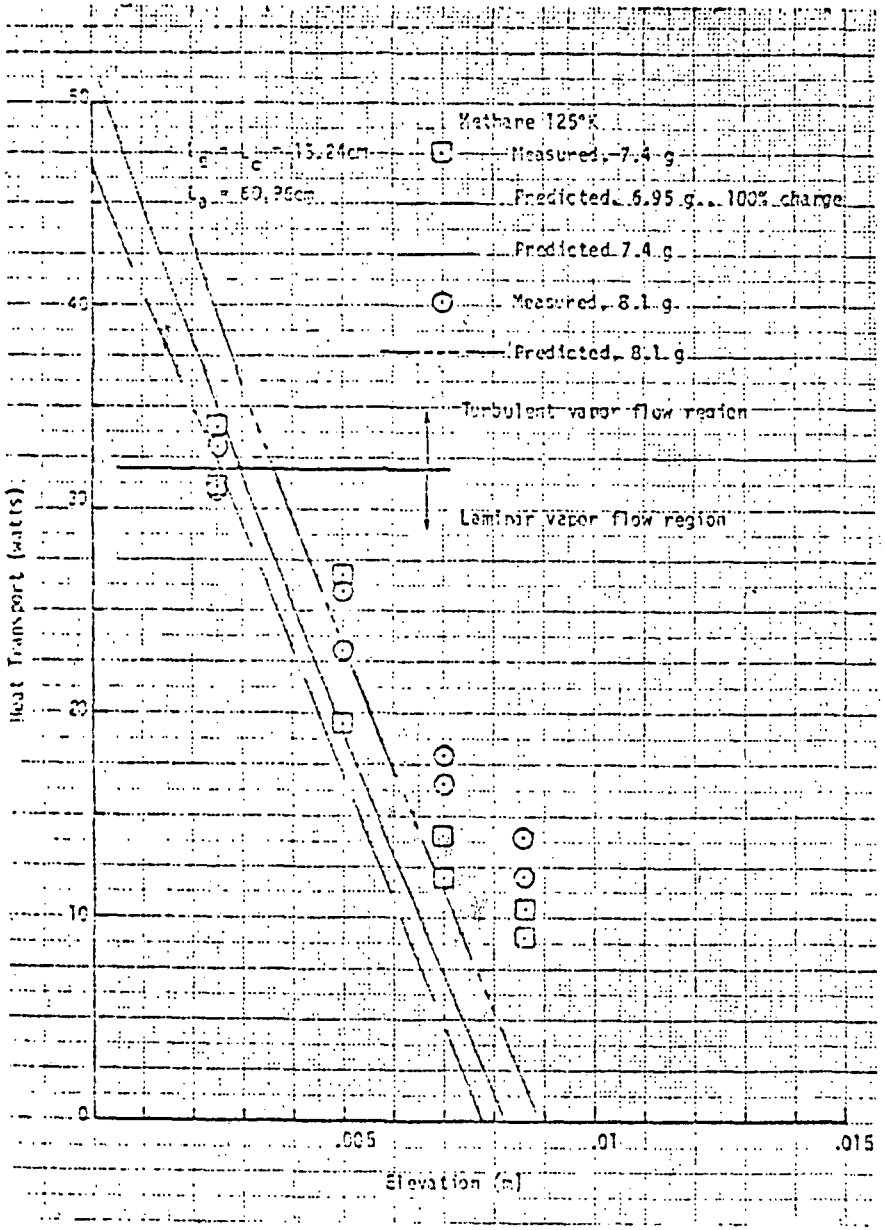

Fig. 3-10 HEAT TRANSPORT AS A FUNCTION OF ADVERSE

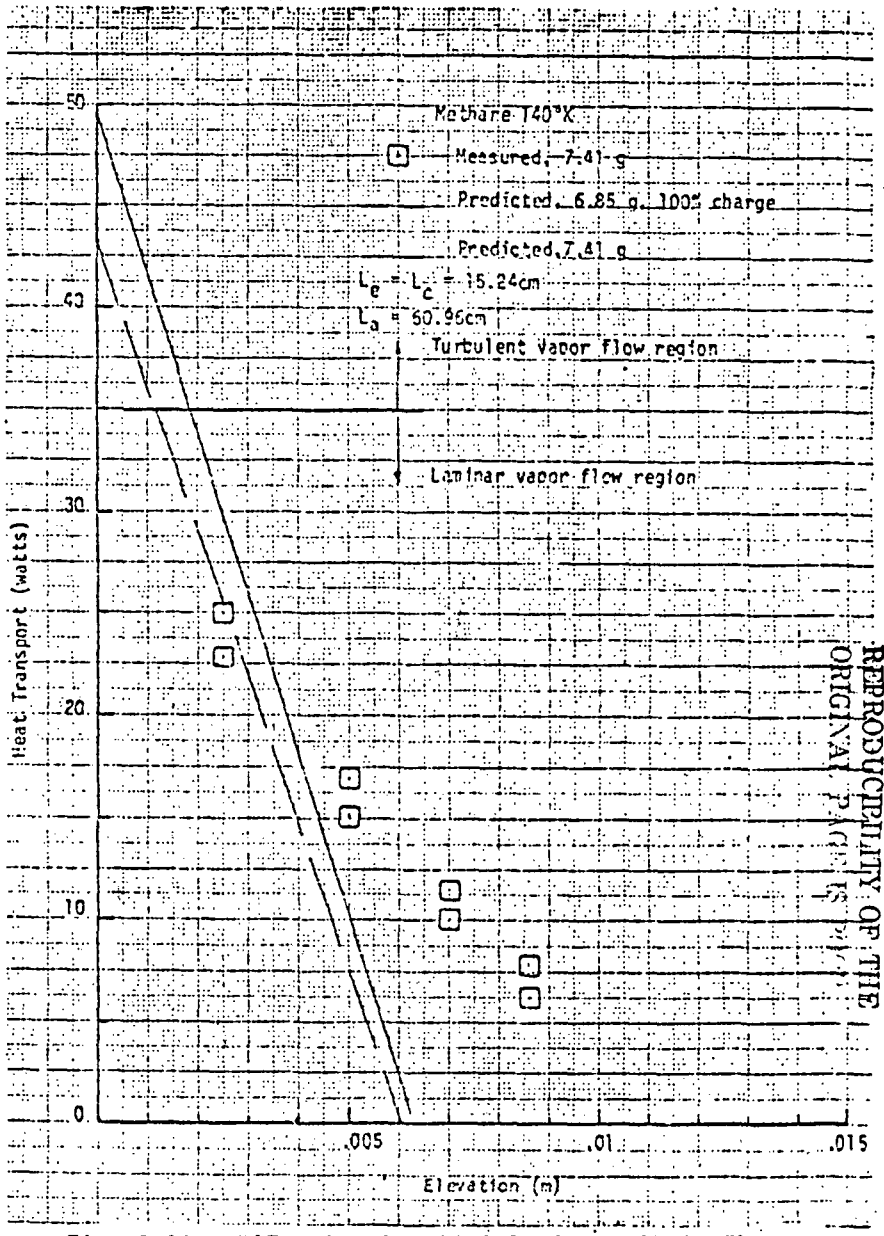

Fig. 3-11 HEAT TRANSPORT AS A FUNCTION OF ADVERSE

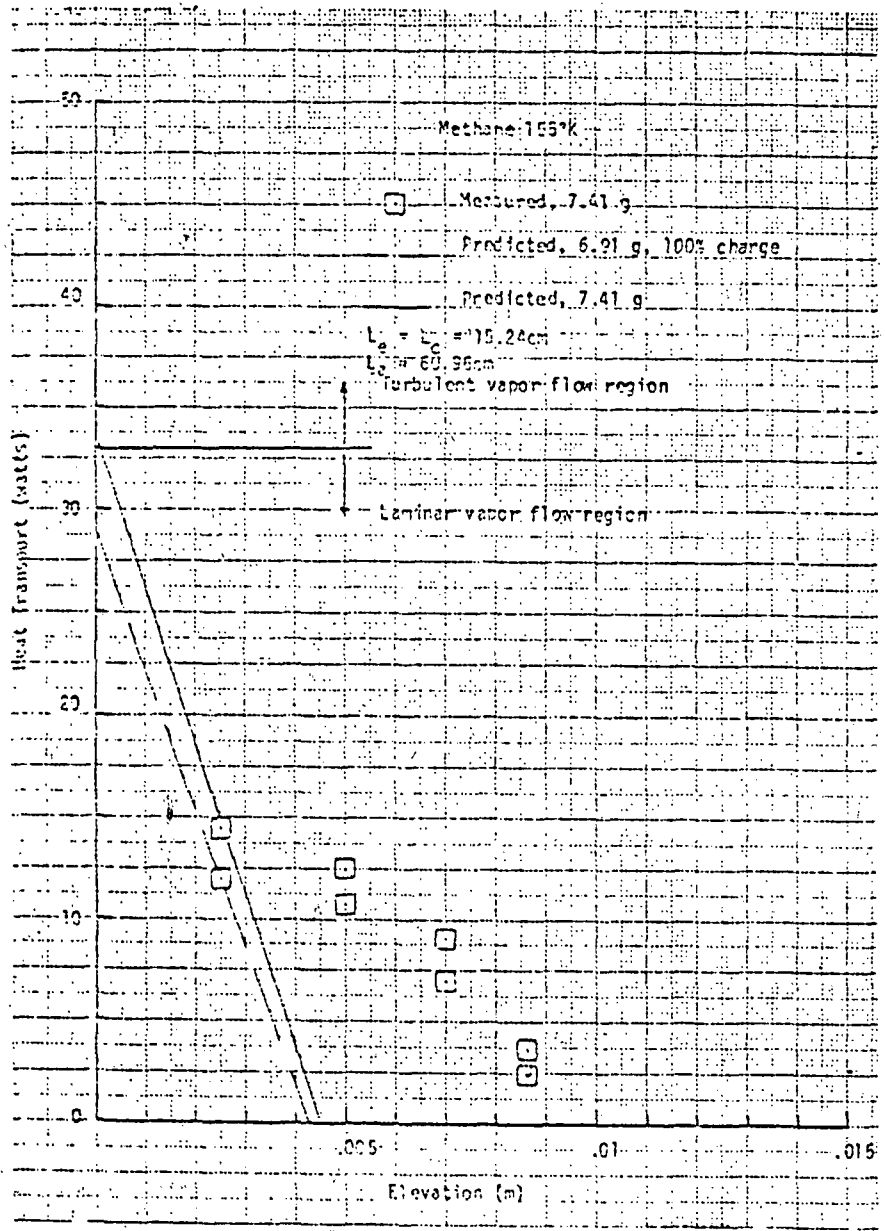

Fig. 3-12 HEAT TRANSPORT AS A FUNCTION OF ADVERSE TILT (METHANE 155°K)

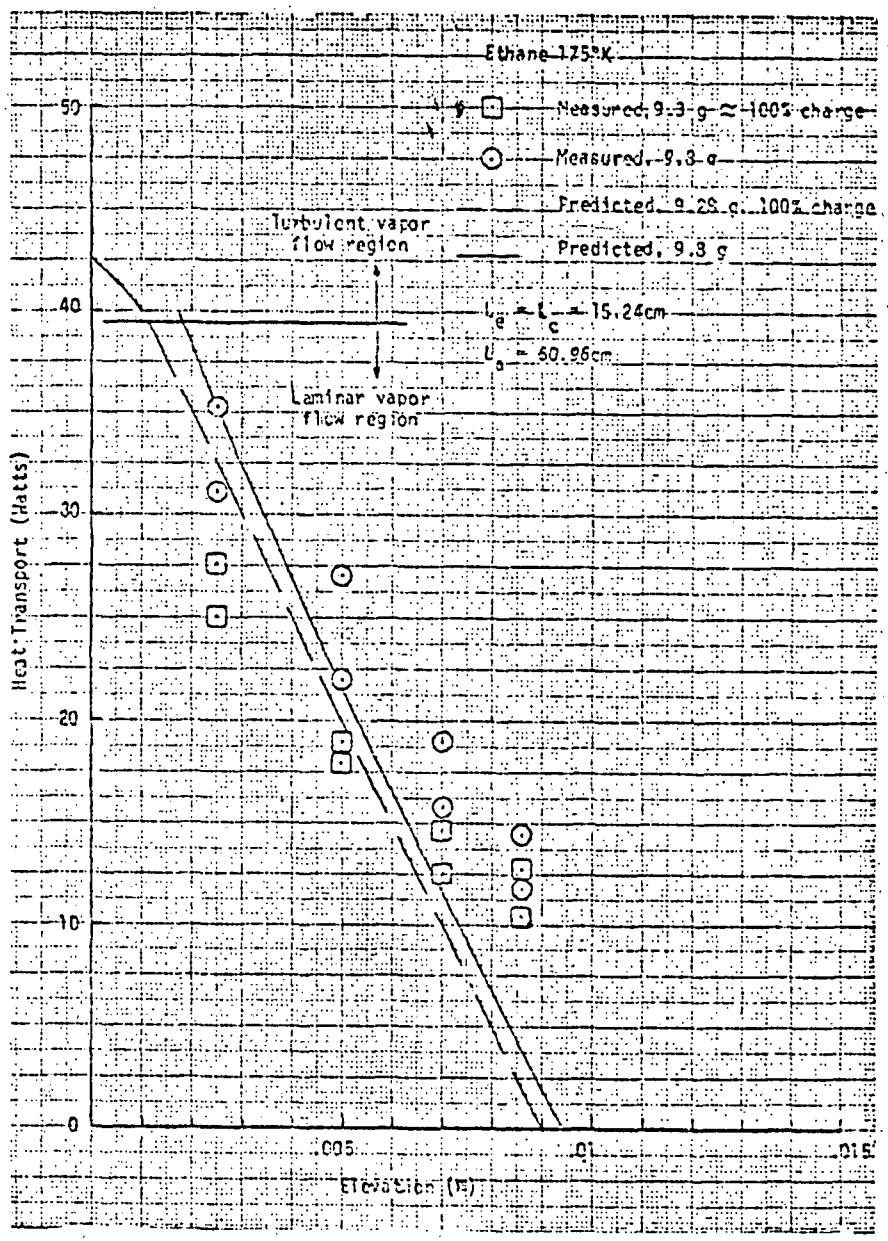

Fig. 3-13 HEAT TRANSPORT AS A FUNCTION OF ADVERSE TILT (ETHANE 175°K)

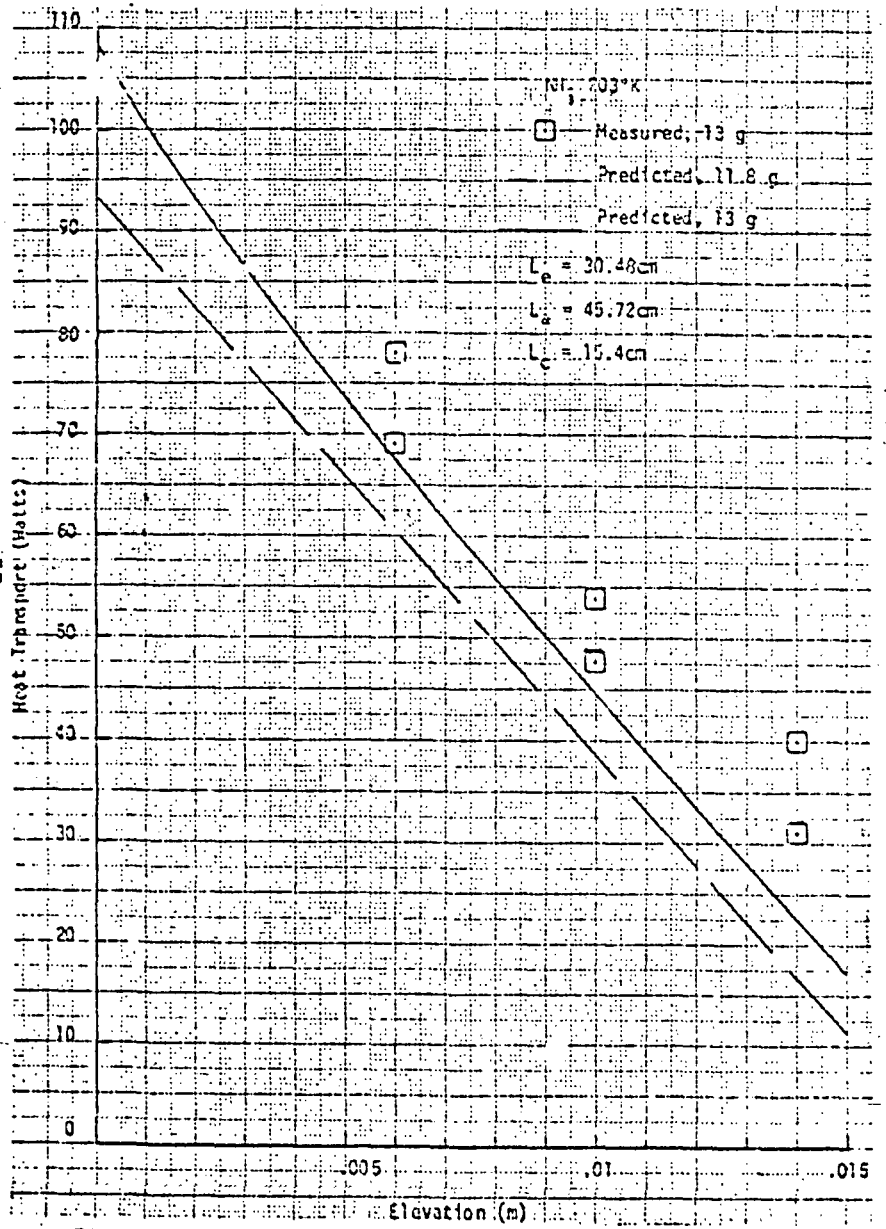

Fig. 3-16 HEAT TRANSPORT AS A FUNCTION OF ADVERSE TILT (AMMONIA 203°K)

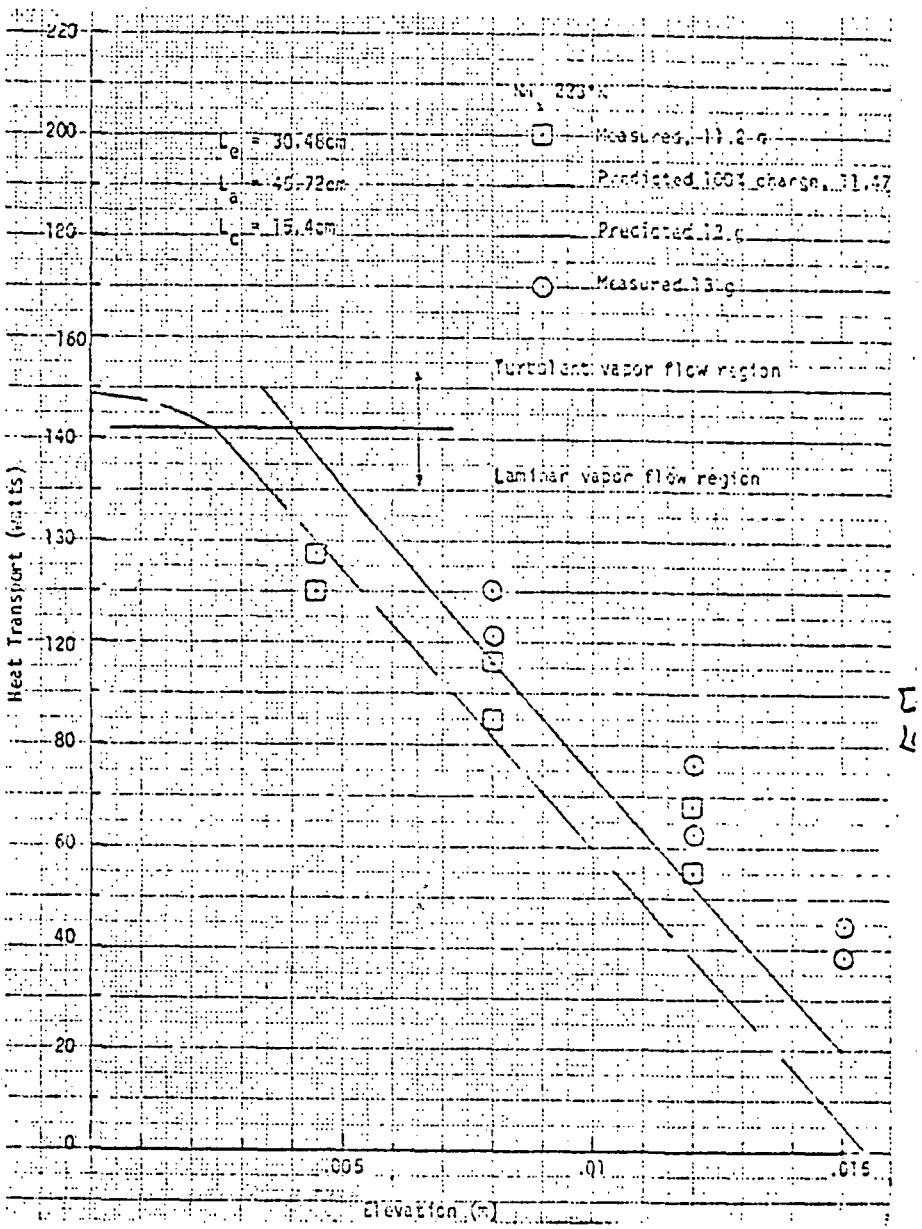

Fig. 3-17 HEAT TRANSPORT AS A FUNCTION OF ADVERSE TILT (AMMONIA 223°K)

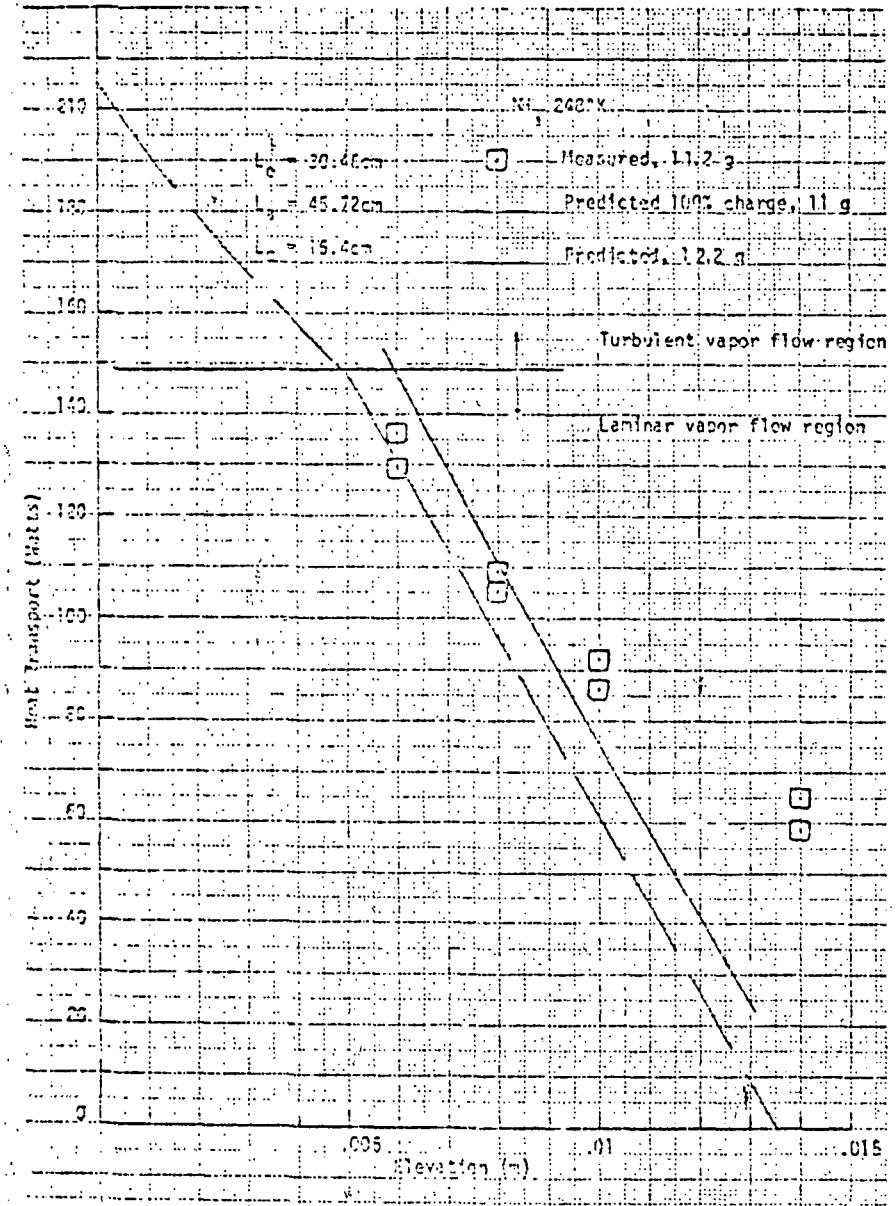

Fig. 3-18 HEAT TRANSPORT AS A FUNCTION OF ADVERSE TILT (AMMONIA 248°K)

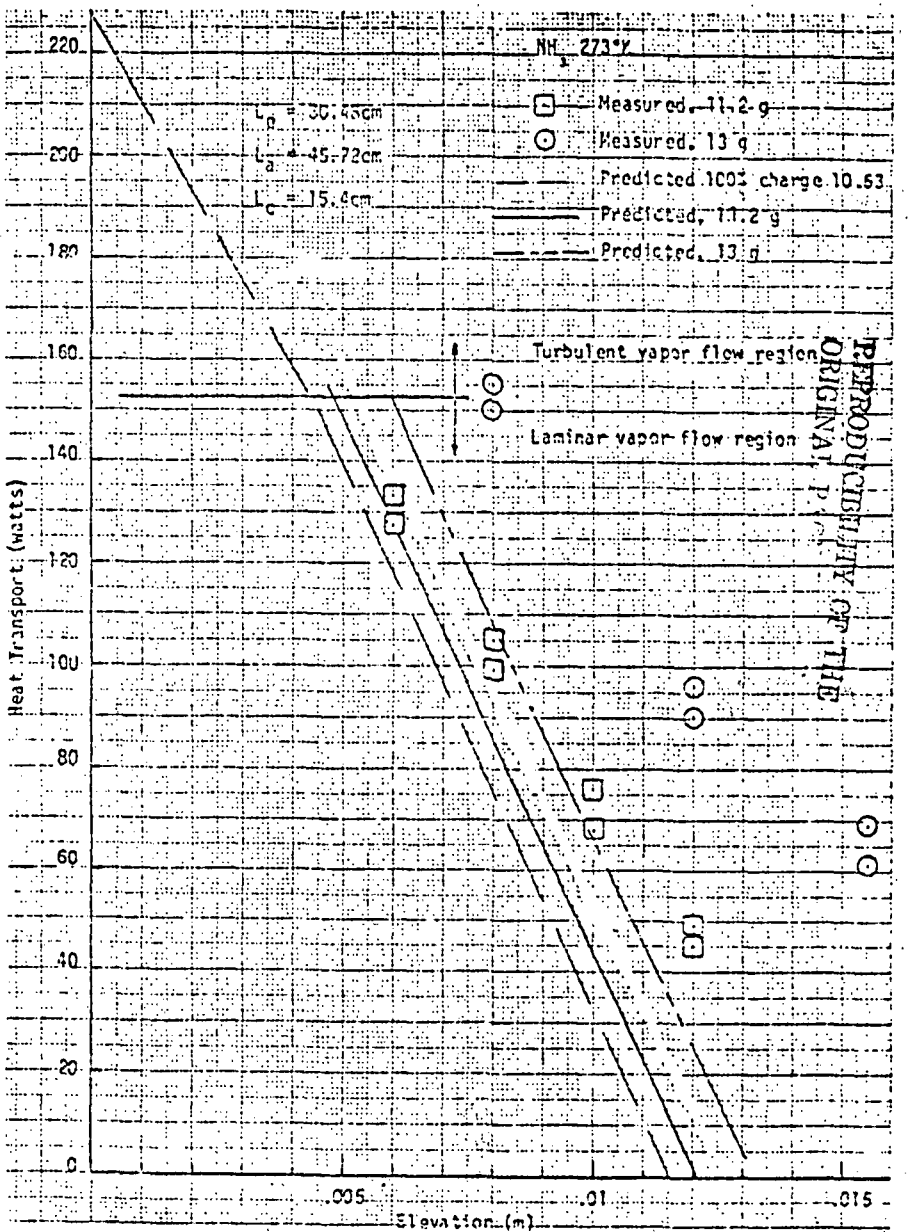

Fig. 3-19 HEAT TRANSPORT AS A FUNCTION OF ADVERSE TILT (AMMONIA 273°K)

the performance; this discrepancy is attributable to the drainage effect. At 273°K, Fig. 3-19, the results for the 11.2 g inventory follow the same performance patterns as predicted for other temperatures, however, the prediction for 13 g (120% charge) shows a significant discrepancy from the measured values; the discrepancy may be due to the following:

1. Error in the data: Based on the measured data of ammonia at 223°K (Fig. 3-17), and methane at 110° and 125°K (Figs. 3-9 and 3-10), it is doubtful that an additional 0.8 g over 12.2 can contribute 50 watts difference in performance. It is possible that the indicated heat pipe elevations are in error.
2. Effects of high overcharge: The 13 g inventory represents a 20% overcharge which is substantially larger than for any other tests and which may have contributed to the higher performance.

3.6.2 Drainage Evaluation

Because of the substantial differences at high elevations, the potential effects due to drainage were investigated. The approach taken was to superimpose a partial drainage condition on the top grooves and then to predict the performance of the bottom grooves using the puddle program. Once the elevation of the pipe exceeded the static height of the individual groove, the top grooves were allowed to drain in proportion to the excess height. The puddle formed by the fluid drainage was calculated and its effect on the remaining grooves was determined. Results are shown in Fig. 3-20. As can be seen, the predicted static elevation due to drainage and puddle flow shows good agreement with the measured values. As the elevation is decreased below this static elevation, measured values tend to be increasingly higher than those predicted. This is due to the fact that the analysis only accounted for static drainage. Because the top grooves

cannot handle any heat, however, dry-out would account for further drainage, thus increasing the capacity of the bottom grooves. A thermal nodal network model will be required to account for this effect.

3.6.3 Fluid Inventory Evaluation

Fig. (3-21) compares the predicted performance as a function of charge at different elevations with the experimental data reported in Ref. 28. The ideal charge was 19 gm. The difference between predicted and measured performance for underfill conditions may be explained by the fact that 27 uniformly filled grooves are assumed in the computer model. For ideal charge, sufficient liquid is available to satisfy all grooves; maximum performance is achieved in each groove and hence good agreement is obtained between predicted and measured performance. For underfill conditions however, there may be nonuniform liquid distribution within the heat pipe which causes some of the grooves to be partially empty while other grooves are completely filled. This could result in a higher performance than predicted for 27 uniformly filled grooves. The non-uniform liquid distribution may be the result of non-uniform groove geometry or possibly different gravity stressing among the top and the bottom grooves.

For overcharge conditions exact correlation is obtained at 2.54 mm (0.1 inches) elevation. The theoretical model overestimates the heat transport as the elevation is increased. At 7.65 mm the measured data is 25 W versus 29.3 W theoretical. This relatively small 4 W difference may be due at least in part to the fact that the burn-out data is probably only accurate to within a few watts.

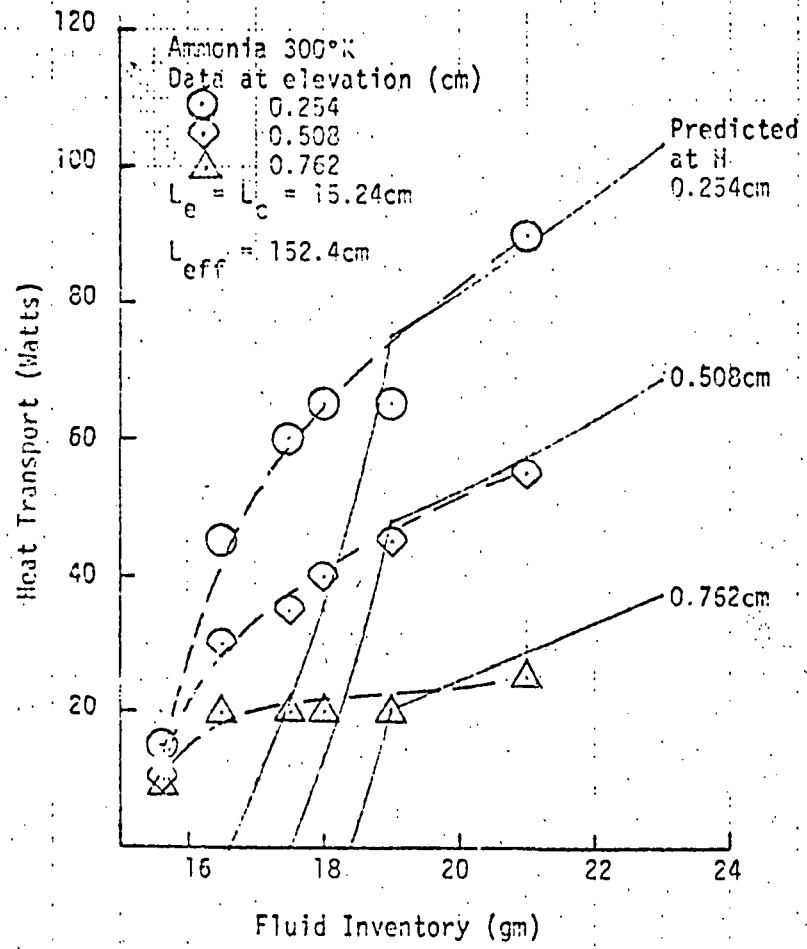

Fig. 3-21 EFFECTS OF FLUID INVENTORY ON HEAT TRANSPORT

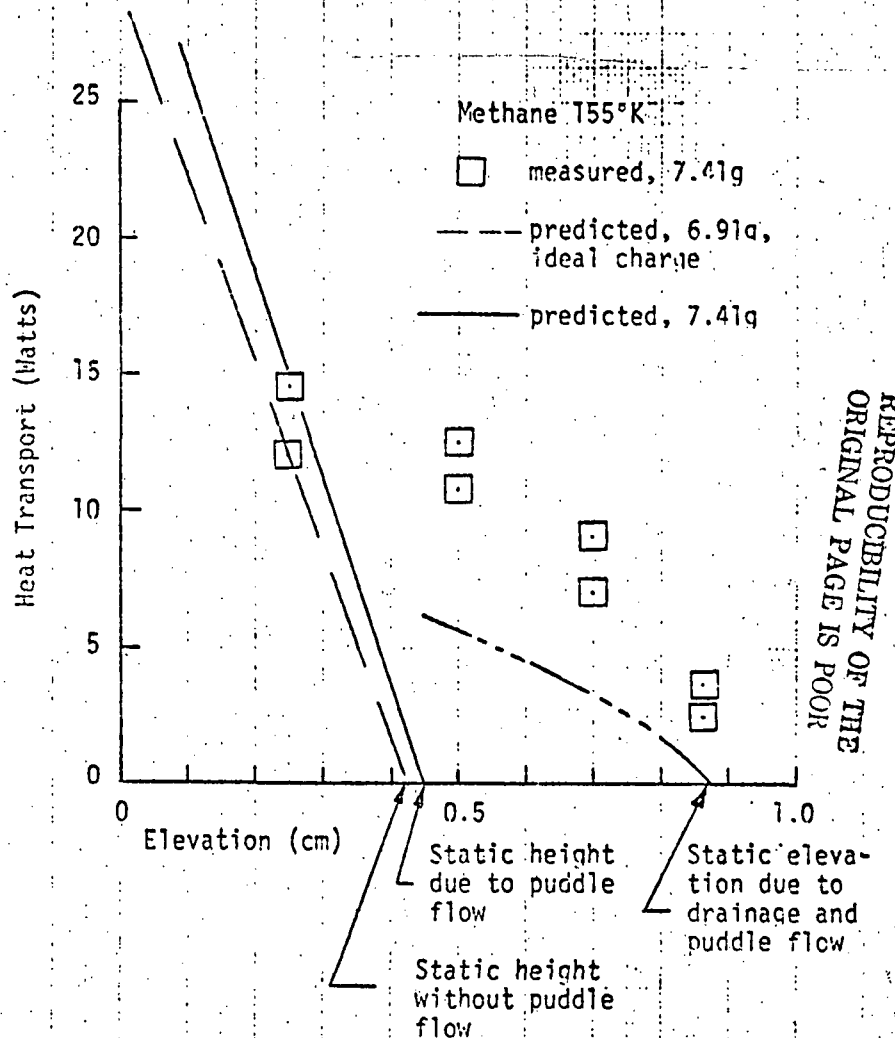

Fig. 3-20 DRAINAGE EFFECT ON PERFORMANCE

4.0 GROOVE DESIGN OPTIMIZATION

4.1 Introduction

The objective of the groove optimization was to establish a procedure for obtaining an axially grooved geometry which will yield the maximum performance for a specified static height, self-priming requirement heat pipe envelope, working fluid, and operating temperature. Groove characteristics as they affect fabricability are included as part of the optimization. To achieve the above mentioned objectives an analytical tool is required to predict the heat pipe performance in the design process The approach taken was to develop a simplified model and determine the parameters dictating the performance. For this purpose a closed form solution was derived under the assumption of laminar flow conditions. Once a design is selected the Groove Analysis Program (GAP) can be used to refin the performance predictions. A detailed description of the derivation of the empirical equation used to predict the capillary pumping limit is presented in Appendix B. The parameters governing the heat pipe performanc were identified in the empirical equation. The significance of these parameters on the performance behavior will be discussed in greater detail. A comprehensive example of the optimization procedure will be presented for the divergent groove which is a preferred design in axially grooved heat pi

4.2 Groove Capillary Flow Factor

The differential Eqs. (3-20) and (3-21) can be reduced to a closed form solution if laminar flow is assumed and the effect of meniscus recessi on liquid flow characteristics can be reduced to an averaged form. For thi purpose an empirical value was developed for the effect of meniscus recessi on capillary pumping and groove characteristics for the divergent groove fo

Both circular and trapezoidal (e.g. Lewis covert groove (Ref. 22) and ATS extruded tubing, respectively) grooves were evaluated. The capillary flow factor can be defined as:

$$N_g = \int_{\frac{1}{2}W}^{\infty} \frac{K_x A'_{\ell x}}{R_x^2} \, dR_x \qquad (4\text{-}1)$$

It can be shown that N_g of a divergent groove with a sharp "land-tip" corner depends on parameters A'_ℓ/W, WP/W and W. A plot of $\frac{N_g \, WP^2}{W^5}$ versus A'_ℓ/W for divergent grooves yields an empirical function:

$$N_g = 0.87 \left\{ \frac{A'_\ell}{W^2} \right\}^{3.1} \left\{ \frac{W}{WP} \right\}^2 W^3 \qquad (4\text{-}2)$$

where A'_ℓ and WP are the groove area and the wetted perimeter respectively, associated with filled grooves with a flat meniscus.

For divergent grooves with round land-tip corners the groove flow factor depends on an additional parameter R_t/W. The following empirical equation was developed:

$$N_g = \left(0.87 - 1.04 \frac{R_t}{W}\right) \left(\frac{A'_\ell}{W^2}\right)^{\left\{3.1 + \frac{2 R_t}{3 W}\right\}} \left(\frac{W}{WP}\right)^2 W^3 \qquad (4\text{-}3)$$

where $0 \leq R_t/W \leq 0.4$ and $WP = \frac{1}{2} (WP_{max} + WP_{min})$

The above groove flow factors were based on an infinite radius of curvature at the downstream end of the condenser. When the meniscus at the downstream end of the condenser is chosen equal to the vapor core radius R_v instead of a flat meniscus, a correction term is required for the groove flow factor. The correction term usually amounts to a 5 to 10% decrease in N_g.

4.3 Empirical Equations for Capillary Pumping Limit

On the basis of the groove capillary flow factor as derived above the governing equation (see Eq. 3-20) for the capillary pumping limit can be developed into a closedform (see Appendix B) for a laminar vapor flow condition as:

$$\frac{QL_{eff}}{R_i^3 N_L} = \frac{N N_g \left\{ 1 - \frac{h}{H} \frac{W}{2} \right\}}{R_i^3 \left\{ 1 + \frac{\nu_v}{\nu_\ell} (f_v + f_{\ell v}) \right\}} \qquad (4\text{-}4)$$

where

the liquid vapor shear parameter is

$$f_{\ell v} = \frac{N}{3\alpha\pi} \frac{A'_\ell}{W^2} \left\{ \frac{R_i}{W} - \alpha \right\}^{-3} \qquad (4\text{-}5)$$

the viscous vapor parameter is

$$f_v = \frac{4}{\pi} \frac{NN_g}{\left\{ \frac{R_i}{W} - \alpha \right\}^4 W^3} \qquad (4\text{-}6)$$

and, wicking height factor is

$$H = \frac{\sigma}{\rho_\ell g} \qquad (4\text{-}7)$$

Eq. (4-4) is in dimensionless form with the right hand side consisting of the following dimensionless parameters:

a. R_i/W, the ratio of heat pipe inside radius to the characteristic width of the groove (W) which is associated with the static height requirements. Therefore, it denotes the dimensionless heat pipe internal radius.

b. α, groove aspect ratio which is a measure of groove depth with respect to the characteristic width of the groove. α, therefore, denotes the dimensionless groove depth.

c. A_ℓ/W^2, dimensionless groove area. It is equal to α for the rectangular groove. Therefore, the deviation of A_ℓ/W^2 from α is an indication of groove obesity.

d. WP/W, dimensionless groove wetted perimeter.

e. f_v, a geometrical parameter which is the ratio of viscous vapor to liquid pressure losses across the heat pipe.

f. $f_{\ell v}$, a geometrical parameter representing the ratio of the liquid/vapor shear to liquid pressure losses.

g. ν_v/ν_ℓ, kinematic viscosity ratio which is the only fluid property on the right hand side of Eq. (4-4). The larger the ratio the higher the vapor and liquid/vapor shear losses. This ratio is normally less than 40 for cryogenic and ambient fluids.

h. $\frac{h\,W}{H\,2}$, this parameter indicates the degradation of transport capability as a result of 1-g operation and heat pipe elevation.

4.4 Composite Factor

Eq. (4-4) places no limit on the size of the groove area that can be used in combination with the groove width. However, it is well known that a composite effect will result if the groove area is made large enough with respect to the groove width. To account for this condition in the groove design, a composite factor S is introduced and defined as the ratio of capill pumping capability when the groove is filled to that obtained when the pipe is priming

$$S \equiv \frac{\Delta P_w}{\Delta P_a} \qquad (4\text{-}8)$$

The numerator is the pumping derived from the groove opening, whereas the denominator is associated with the groove hydraulic radius depending on the groove area and wetted perimeter that is developed during priming.

Based on the above definition, Eq. (4-8) can be rewritten in terms of the groove geometric properties as follows:

$$S = \frac{A_\ell'/WP}{W/2} = \frac{2\,A_\ell'}{WP\,W} \qquad (4\text{-}9)$$

The formulation of Eq. (4-9) can also be interpreted in terms of the static height capabilities of the heat pipe in 1-g operation. By multiplying and dividing the middle term of Eq. (4-9) by $\frac{\sigma}{\rho_\ell g}$ one has:

$$S = \frac{\frac{\sigma}{\rho_\ell g}\,\frac{2}{W}}{\frac{\sigma}{\rho_\ell g}\,\frac{WP}{A_\ell'}} = \frac{h_w}{h_s} \qquad (4\text{-}10)$$

where h_w is the static height capability developed by the groove opening when the pipe is filled, whereas h_s is that obtained during the self-priming mode. If the composite factor is greater than unity the groove can not prime itself in the range of static height h_s to h_w. In this case one has to allow the heat pipe to prime statically at an elevation less than h_s under a heat load greater than zero and less than the heat pipe transport capability.

Substituting Eq. (4-9) into (4-2) yields:

$$N_g = \frac{0.87}{4}\,S^2\left\{\frac{A_\ell'}{W^2}\right\}^{1.1} W^3 \qquad (4\text{-}11)$$

Combining Eqs. (4-11) and (4-4) one can see that the larger the composite factor, the higher the heat pipe performance until the vapor and liquid vapor shear losses become dominant.

4.5 Heat Pipe 1-g Performance Evaluation

A characteristic of most heat pipes operating in the cryogenic to ambient temperature range is that they are mostly liquid flow limited. To optimize the performance, therefore, it is desirable to provide large flow channels, to minimize viscous losses in combination with a small pumpin pore size to maximize capillary action. In addition, it is also desirable t provide the maximum number of flow channels consistant with vaopr flow restr tions.

In the absence of body forces, i.e. "o-g", there are no constraints on groove width (W) except vapor flow and fabrication limits. Any heat pipe, however, must be tested on the ground to verify performance. Since capillary forces are relatively weak compared to gravity, ground test conditions become the primary constraint on the size of the groove width opening. The need to optimize the groove design for a nominal test elevatio is evident from Figs. 3-8 through 3-19. For both high and low elevations measured data deviates from predicted performance. Axially grooved heat pipes therefore, should be designed to provide optimum performance around a nominal test point. It is also evident from the test data presented in those figures that the higher the test elevation, the wider the band of reliable test data. The axial groove heat pipe, therefore, should be designed with a groove width whose corresponding static height is about 1.5 2.0 times the nominal test elevation. In addition the optimum performance should be accomplished at the nominal elevation.

Referring to Eq. (4-11), it can be seen that for a given composite factor and groove geometry, the groove capillary flow factor is proportional to (W^3) since the ratio (A'/W^2) is approximately constant. The larger the

groove width W, the higher the groove capillary flow factor. By substituting Eqs. (4-11) into (4-4) and assuming insignificant vapor and liquid/vapor shear losses, one realizes that the heat pipe performance at a fixed elevation, h_t, will be maximized at an optimum groove width. The optimum groove width can be readily obtained with the approach of differentiating the dimensionless performance $\frac{QL_{eff}}{R_i N_L}$ with respect to the groove width. During the differentiation one further assumes that the composite factor and the groove form are invariant. The result shows that for $\delta/R_i \leq .25$ the optimum groove width (W_{opt}) should be $\frac{W_{opt}}{H/h_t} = 1.25 - 1.33$, which in turn indicates $h_{max}/h_t = 1.5 - 1.6$. The groove characteristic of $\frac{W}{R_i/\alpha} = \frac{\delta}{R_i}$ is usually less than 0.5 which is equivalent to $h_{max}/h_t = 2.0$.

Based on the above analysis the criterion for obtaining the groove opening is to determine its corresponding static height, h_{max}, in the range of .5 to 1.0 times greater than the specified test elevation. In this case one can have the optimum performance and a wider band of testable elevation in the neighborhood of the specified test elevation.

4.6 Parametric Analysis for Divergent Grooves

This section presents the predicted performance of both circular and trapezoidal divergent grooves (Fig. 4-1) based on the theory developed in Sections 4.2 through 4.4. The typical performance of circular divergent grooves is shown in Figs. 4-2 through 4-4 for $R_i/W = 8$ and $t/w = .59$, $R_i/W = 12$ and $t/w = .9$ and R_i/W and $t/w = 1.0$, respectively.

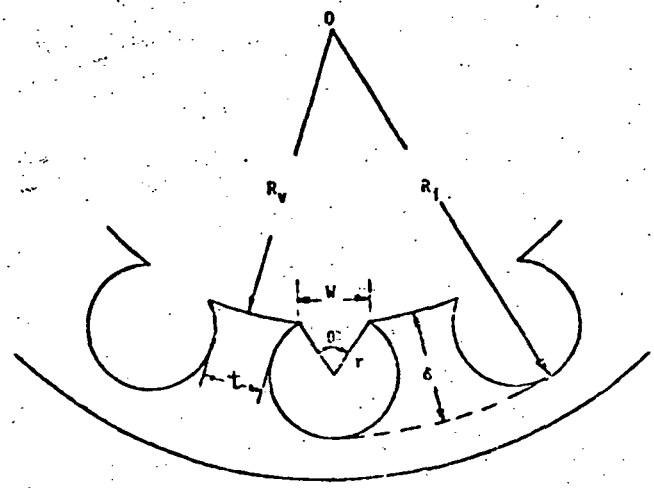

Circular Divergent Grooves

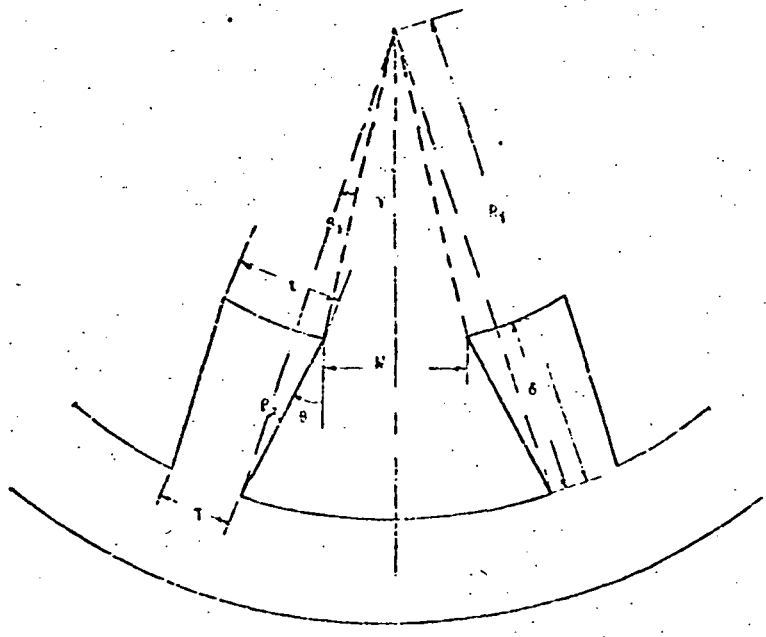

Trapezoidal Divergent Grooves

Fig. 4-1 DIVERGENT GROOVE PROPERTIES

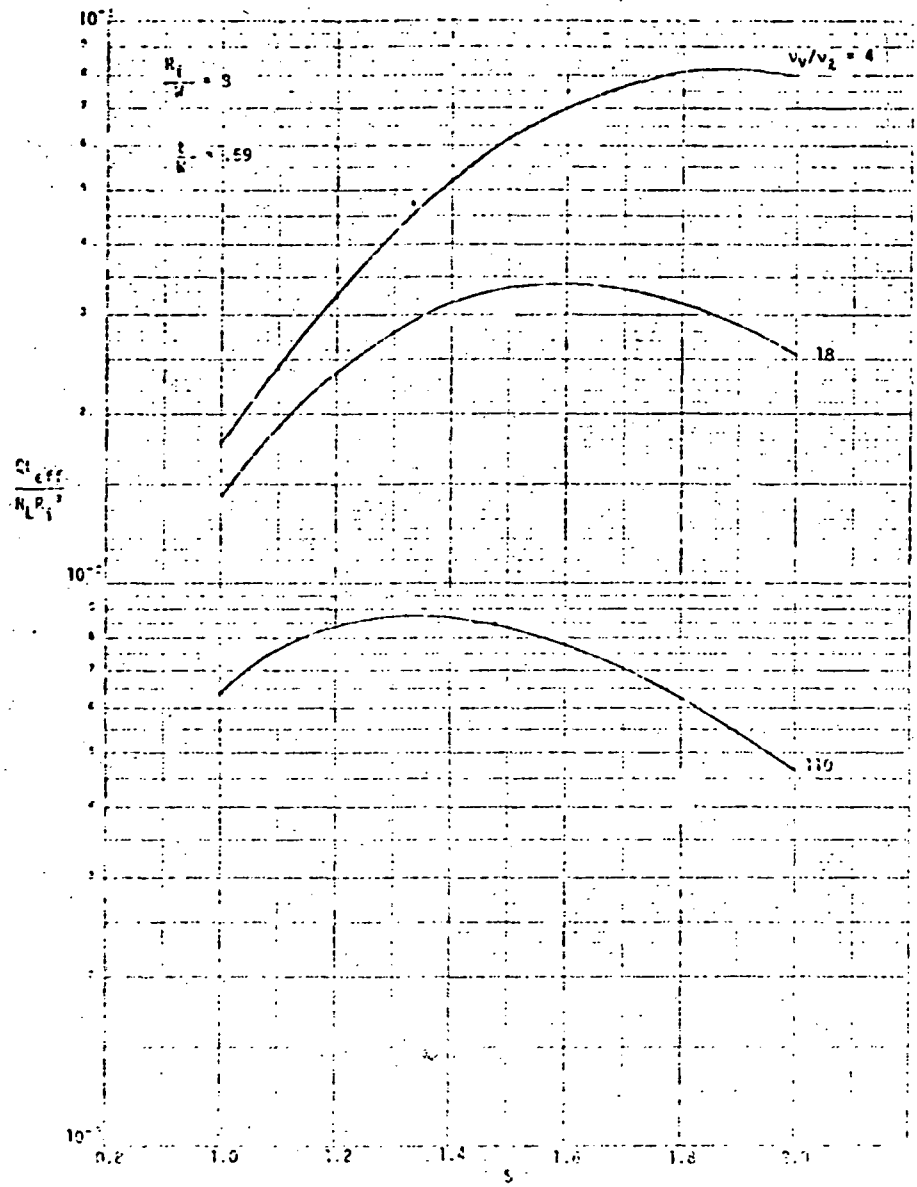

Fig. 4-2 TRANSPORT CAPABILITIES OF CIRCULAR GROOVES ($\frac{R_i}{W} = 8$)

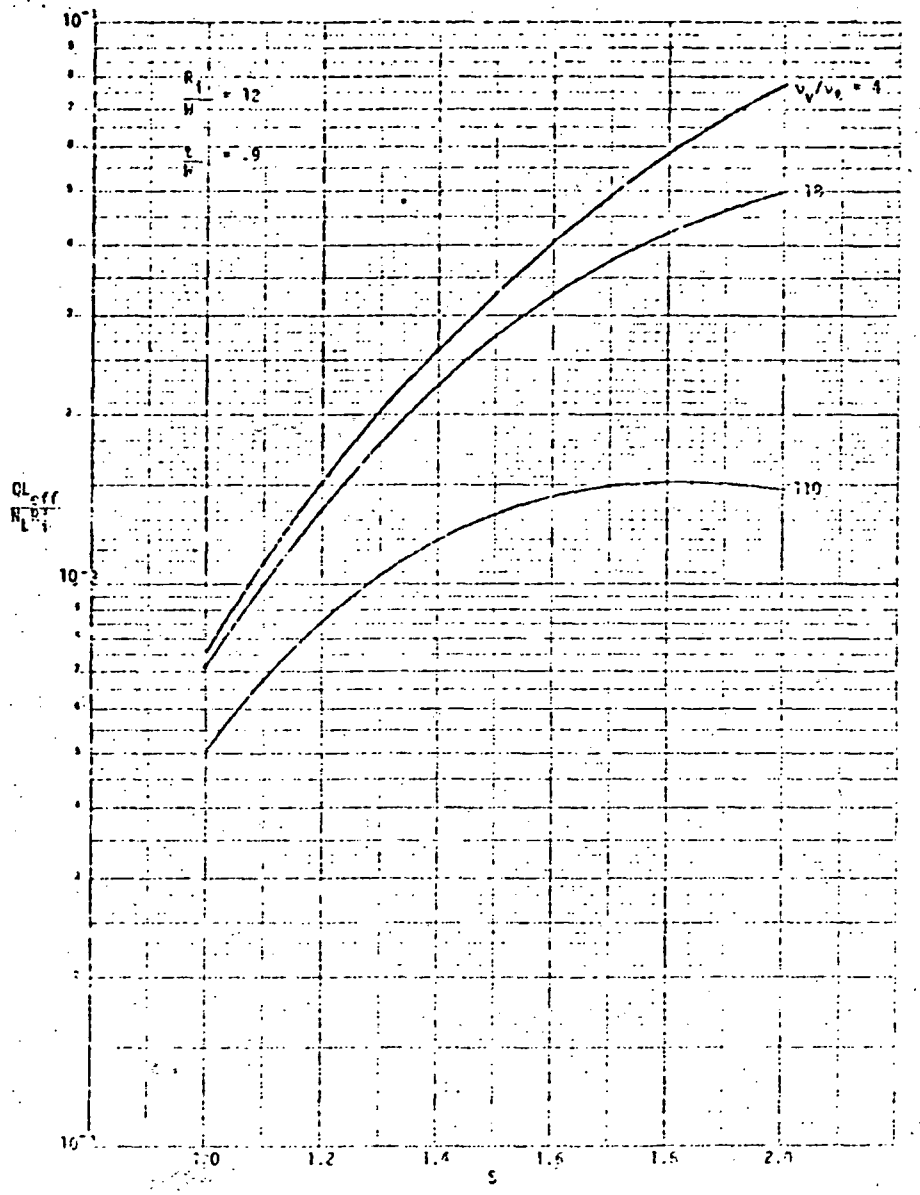

Fig. 4-3 TRANSPORT CAPABILITIES OF CIRCULAR GROOVES ($\frac{R_i}{W} = 12$)

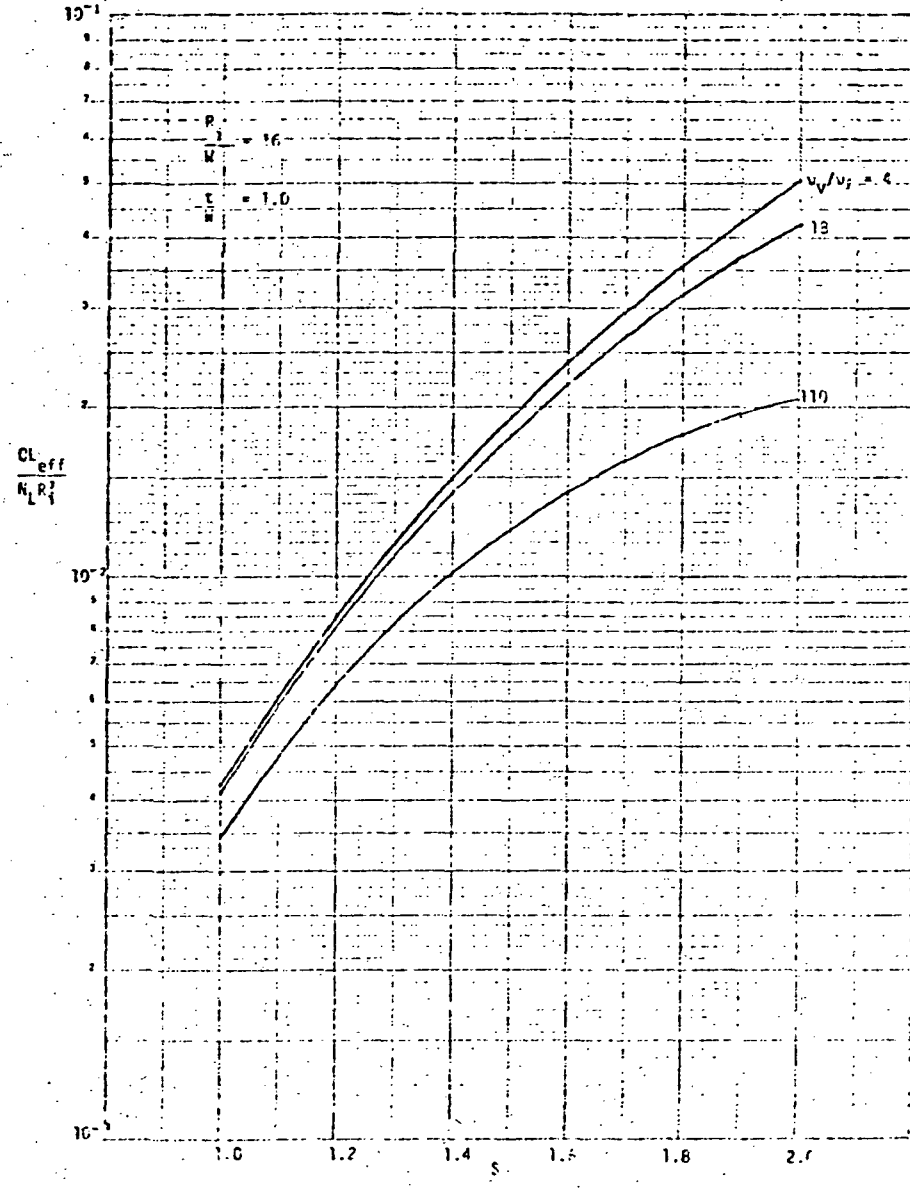

Fig. 4-4 TRANSPORT CAPABILITIES OF CIRCULAR GROOVES ($\frac{R_i}{W} = 16$)

As can be seen in Fig. 4-2, a maximum point of performance is achieved for each value kinematic viscosity (or operating temperature) beyond which lower performance results as the composite factor is increased. The maximum is achieved at different composite factors for different kinematic ratios. The performance behavior shown in the figure results from the combination of the following factors as the composite factor is increased:

a. The decreasing number of grooves within the heat pipes.

b. The increasing groove flow factor N_g of each groove due to increasing groove area.

c. The increasing vapor viscous and liquid/vapor shear losses due to a smaller vapor core diameter

As the parameter R_i/W increases the maximum performance occurs at a higher composite factor and the effect of vapor viscous and liquid/vapor shear losses becomes less pronounced.

Figs. 4-5 through 4-10 show the o-g performance of trapezoidal grooves. The discontinuity in the slopes of the performance curves of Fig. 4-5 through 4-7 results from the application of the land thickness criterion. The location of the discontinuity corresponds to uniform land thickness. The discontinuity in the performance slope for S = 1.25 was not shown in Figs. 4-8 through 4-10 since it occurred at higher groove aspect ratios. The transport capability of circular grooves is also shown in these figures for comparison. Since the groove aspect ratio and the composite factor are interdependent parameters in circular grooves, one can only obtain a particular circular groove form for given criteria of R_i/W, land thickness, and composite factor. In comparing the performance of circular grooves with trapezoidal

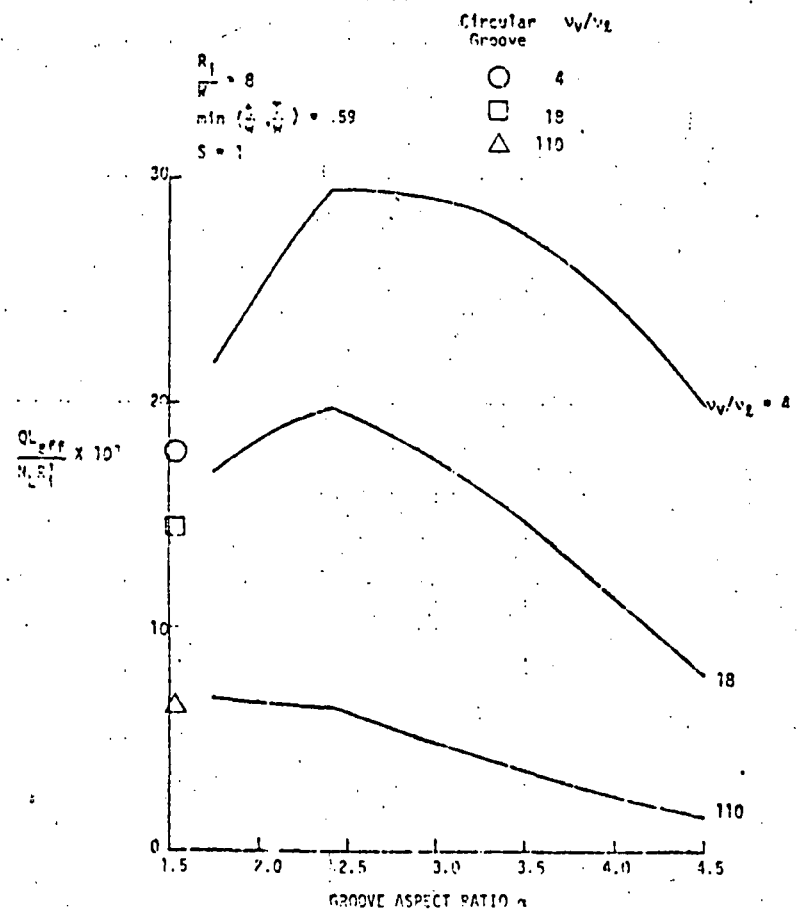

Fig. 4-5 TRANSPORT CAPABILITIES OF TRAPEZOIDAL, DIVERGENT GROOVES (S=1, R/W-8)

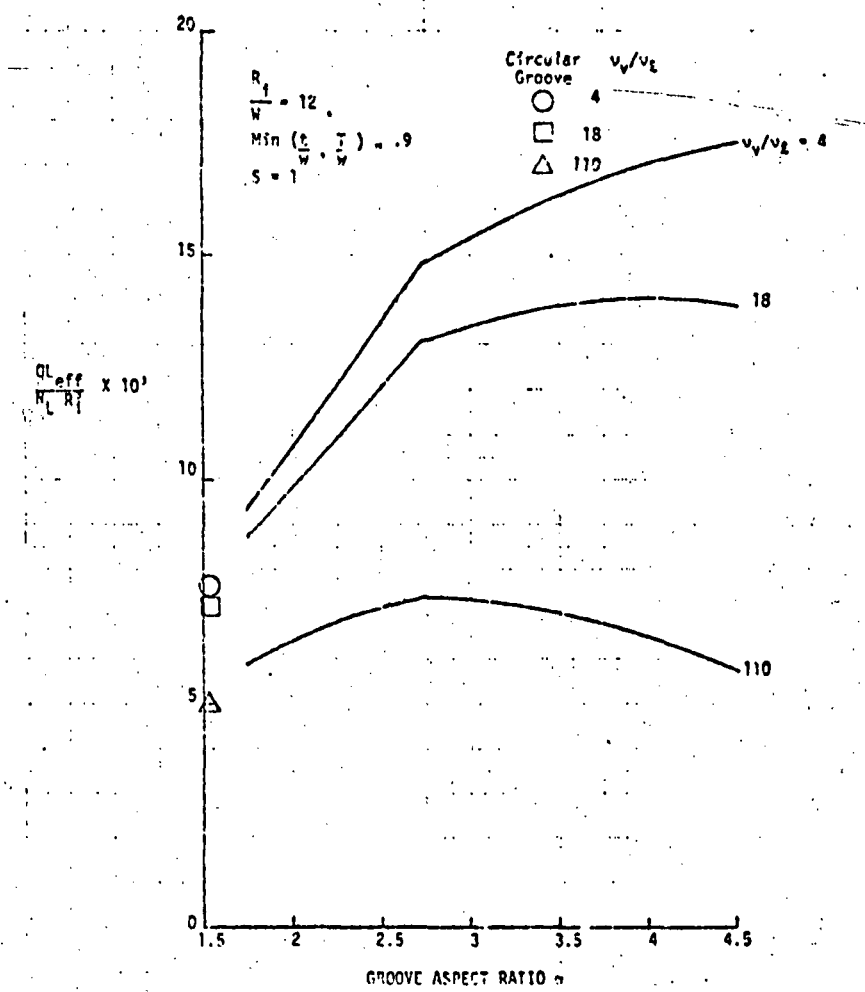

Fig. TRANSPORT CAPABILITIES OF TRAPEZOIDAL, DIVERGENT GROOVES (S=1, $R_1/W = 12$)

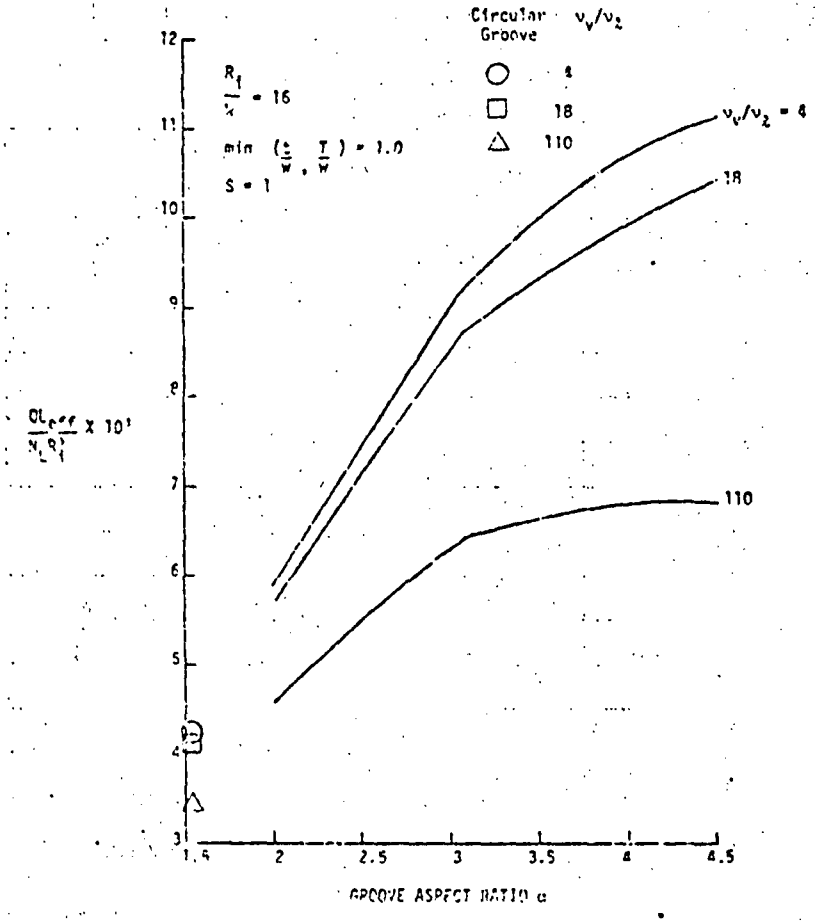

Fig. 4-7 TRANSPORT CAPABILITIES OF TRAPEZOIDAL, DIVERGENT GROOVES (S=1, R_i/W = 16)

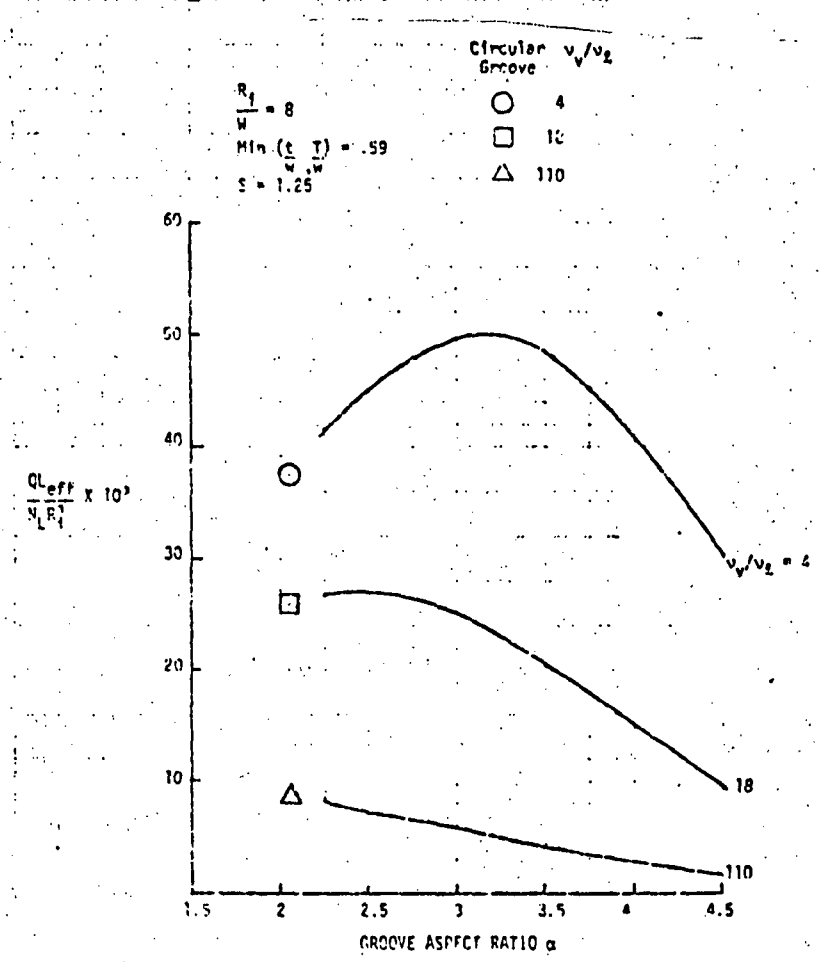

Fig. 4-8 TRANSPORT CAPABILITIES OF TRAPEZOIDAL, DIVERGENT GROOVES (S=1.25, R_i/W = 8)

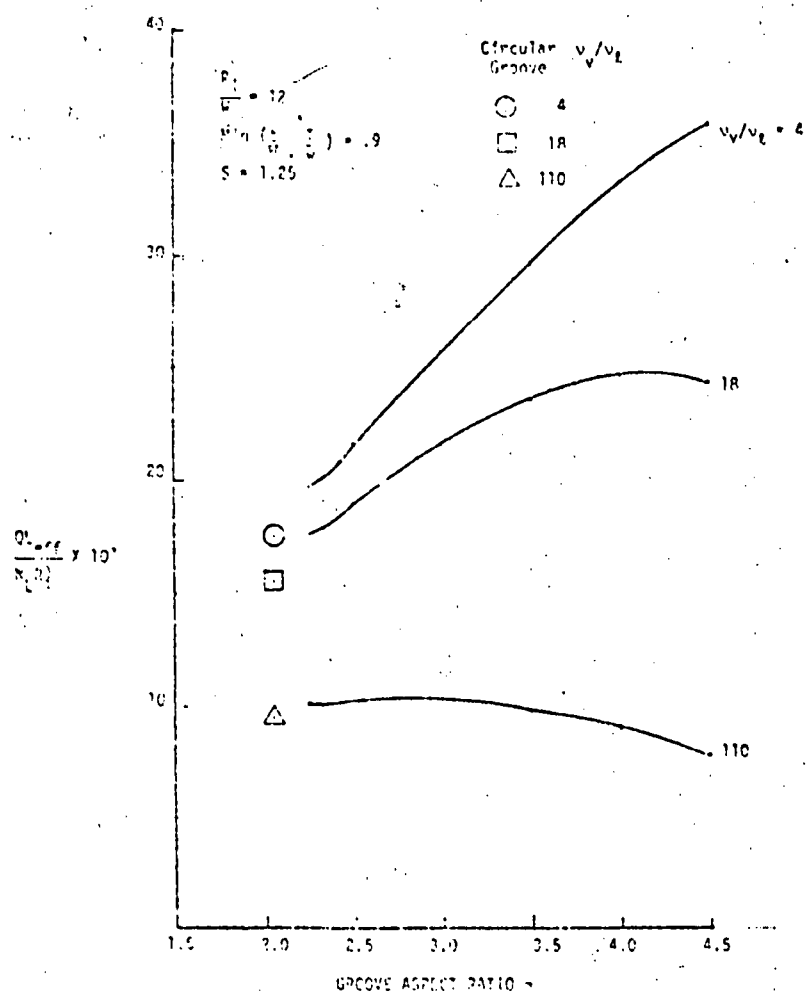

Fig. 4-9 TRANSPORT CAPABILITIES OF TRAPEZOIDAL, DIVERGENT GROOVES (S=1.25, R_j/W = 12)

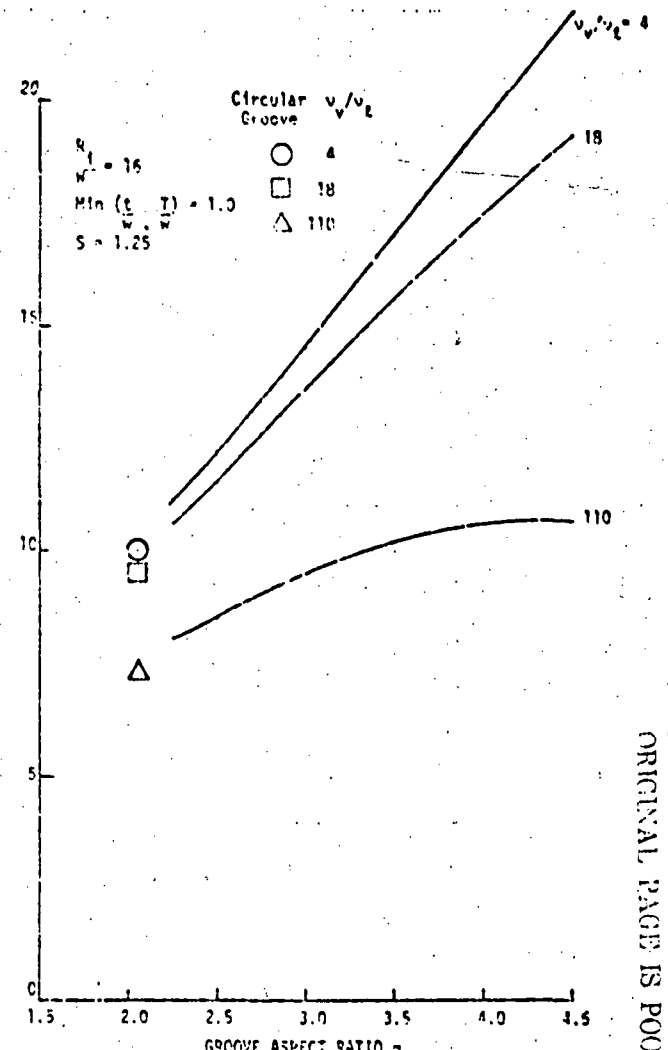

Fig. 4-10 TRANSPORT CAPABILITIES OF TRAPEZOIDAL, DIVERGENT GROOVES (S=1.25, R_j/W = 16)

grooves, one notes that at a given set of R_i/W, land thickness and composite factor, the circular groove performs like a trapezoidal groove of low aspect ratio.

4.7 Improved Groove Design

On the basis of the above optimization analysis, one realizes that the trapezoidal grooves can yield higher performance than circular grooves at the same level of composite factor. In the selection of trapezoidal geometries for axially grooved heat pipes one should also consider the constraints introduced by the fabrication process and the tube material. At the present time no attempt has been taken to include such considerations in the optimization analysis since the formulation of these constraints in terms of groove parameters is not easily obtainable.

To complete the objectives of this study a trapezoidal groove from as shown in Fig. 4-11 is introduced which is comparable in size and groove form to the ATS-6063 extruded tubing. However, the performance is improved significantly. As a typical example, for ammonia at 300°K ($\nu_v/\nu_\ell = 4$), the improved groove form can yield 75% higher heat transport capability and 100% higher static height capability than the ATS groove.

IMPROVED GROOVE PROPERTIES

Number of grooves	$N = 30$
Groove root diameter	$2R_i = 1.092$cm
Groove width	$W = 0.034$cm
Groove depth	$\delta = 0.102$cm
Land thickness	$T = 0.051$cm
Groove divergent angle	$2\theta = 30$ deg.
Groove Composite factor	$S = 1.25$

$$\frac{QL_{eff}}{N_L W^3} = 65 \text{ at } \nu_v/\nu_\ell = 4$$

QL_{eff} for ammonia at 300°K = 270 w-m (10,500 w-in.)

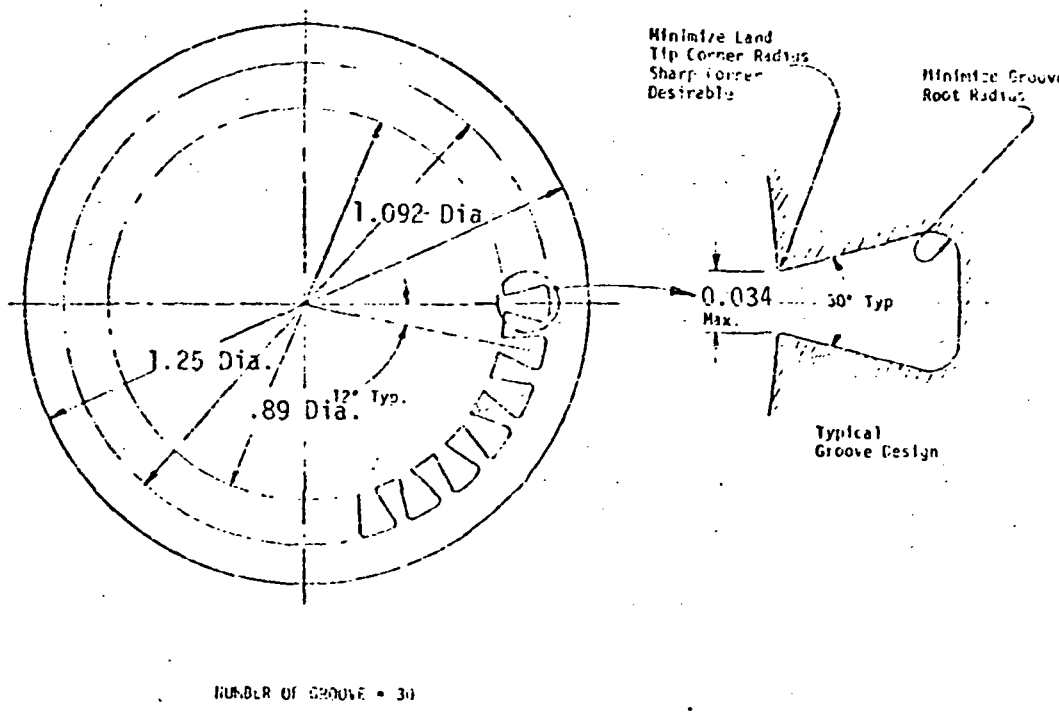

Fig. 4-11 IMPROVED GROOVED DESIGN

5.0 CONCLUSIONS AND RECOMMENDATIONS

The axially grooved heat pipe has been applied to a variety of aerospace systems. The extensive use and reliable performance has demonstrated the versatility of this design. Numerous design and performance requirements have been identified for future space missions utilizing both fixed conductance and thermal control heat pipes. Experience to date indicates that the extrusion process is the best method for producing aluminum axially grooved tubing. For materials other than aluminum, the swaging process is the only known process which can effectively be used today to produce axially grooved tubing on a cost effective basis.

Reduced sensitivity to gravity and increased heat transport capacity can be obtained with the extruded groove forms. Fabrication limitations and sensitivity to composite pumping effects should be investigated. To accomodate future requirements, improved groove form hardware should be developed and performance verified. Development of hardware in materials other than aluminum should also be continued especially low conductivity materials such as stainless steel for TCHP applications. Performance of axially grooved heat pipes with non-condensible gases should also be verified and any degradation mechanisms identified.

Although good agreement with measured data has been obtained with the analytical models developed under this program, continued improvements should be pursued. Turbulent and transition vapor flow regions should be investigated if higher performance heat pipes are to be developed. Liquid/vapor shear effects as a function of groove form and geometry as well as vapor flow conditions should be studied further and analytical models refined accordingly. Additional test

data should also be obtained to verify puddle flow contributions. Finally non-uniform flow conditions including asymmetric heat addition and removal and groove drainage should also be investigated.

6.0 NOMENCLATURE

Symbol	Description
A	Cross-sectional area
A'_ℓ	Area of a single groove with no meniscus recession
D	Diameter
f	Frictional factor, function
g	Gravity
h	Elevation
H	Rise factor, $H = \frac{\sigma}{\rho_\ell g}$
K	Permeability
L	Length
m	Mass flow rate
M	Molecular weight
N	Number of grooves
N_g	Groove capillary flow factor
P, p	Pressure
Q	Total heat input or output
Q_x	Axial heat flow rate
R	Radius
Re	Reynolds number
R_o	Universal gas constant
t	Land thickness at top
T	Temperature, Land thickness at bottom
W	Groove width or opening
WP	Wetted perimeter
X, x	Axial direction

Symbol	Definition
α	Groove aspect ratio.
β	Heat pipe tilt angle.
γ	Ratio of specific heats
δ	Groove depth, angle
θ	Angle, divergent angle
λ	Heat of vaporization
μ	Viscosity
ν	Kinematic viscosity
ξ	Groove land taper angle
ρ	Density
σ	Surface tension
τ	Shear force
ϕ	$\phi = \frac{1}{2\alpha}$
ψ	Liquid/vapor shear parameter

Subscripts	Definition
a	Adiabatic
b	Body Force
c	Condenser
e	Evaporator, entrainment
eff	Effective
g	Groove
h	Hydraulic
i	Internal
ℓ	Liquid
max	Maximum
opt	Optimum
p	Puddle

s	Sonic (Eq. 3-23), Submerged (Section 3.4.2)
sl	slug
t	Land tip corner
v	vapor
$\parallel$	Parallel
$\perp$	Perpendicular

7.0 REFERENCES

1. Kroliczek, E. J. and Brennan, P. J. "Axially Grooved Heat Pipes - Cryogenic Through Ambient," ASME Paper No. 73-ENAS-48, July 1973.

2. Schlitt, R., et al. "Parametric Performance of Extruded Axial Grooved Heat Pipes from 100° to 300°K." AIAA Paper No. 74-724, July 1974.

3. Harwell, W. et al. "Orbiting Astronomical Observator Heat Pipe Flight Performance Data," AIAA Paper No. 73-758, July 1973.

4. Berger, M. E. and Kelly, W. H. "Application of Heat Pipes to the ATS-F Spacecraft," ASME Paper No. 73-ENAs-46, July 1973.

5. McIntosh, R. et al. "Sounding Rocket Heat Pipe Experiment," AIAA Paper No. 72-259, 1972.

6. Ollendorf, S., et al. "Performances of Heat Pipe in Zero Gravity," International Conterence on Heat Pipes, 1973.

7. Edelstien, F., "Deployable Heat Pipe Radiator," Grumman Aerospace Corporation, DHPR-75-13, April 1975.

8. "Transient Thermal Response of a Thermal Control Canister," Final Report, Contract NAS5-22570, prepared for NASA, GSFC by Grumman Aerospace Corporation, Bethpage, N. Y. 1976.

9. Brennan, P. J. and Groll, M. "Application of Axial Grooves to Cryogenic Variable Conductance Heat Pipe Technology," 2nd International Heat Pipe Conference, April 1976.

10. Harwell, W. and Ball, T. "Thermal Vacuum Tests on a Thermal Control Canister Breadboard," Contract NAS5-22980, prepared for NASA, GSFC by Grumman Aerospace Corporation, Bethpage, N. Y. 1977.

11. Jen, H. and Brennan, P. J. "Summary Report for Development of Copper/Water Axially Grooved Heat Pipes for Low Cost High Performance (LCHPG) Applications," BK017-005, B & K Engineering, Inc., September 1976.

12. Sherman, A. and Brennan, P. J. "Cryogenic and Low Temperature Heat Pipe/Cooler Studies for Spacecraft Application," Journal of Spacecraft and Rockets, Vol. 13, No. 5, pp 288-293, May 1976.

13. Wright, J. P. and Pence, W. R. "Development of a Cryogenic Heat Pipe Radiator for a Detector Cooling System," ASME Paper No. 73-ENAs-47, July 1973.

14. Richter, R. "Solar Collector Thermal Power System - Development, Fabrication, and Testing of Fifteen Foot Heat Pipes," Xerox Corporation, November 1974.

15. RCA Advanced Technology Laboratories, "ICICLE Feasibility Study," Final Report, Radio Corporation of America, Camden, N. Y. 1970.

16. Jen, H. F. and Kroliczek, E. J. "User's Manual for Groove Analysis Program (GAP)," BK012-1007, B & K Engineering, Inc. June 1976.

17. Belinas, T. A. and Harwell, W. "Orbiting Observatory Heat Pipes - Design, Analysis and Testing," ASME Paper No. 70HT/SpT-9, 1970.

18. Brennan, P. J. et al. "Arterial and Grooved Cryogenic Heat Pipes," ASME Paper No. 71-WA/HT-42, November 1971.

19. "High-Precision Heat Pipes," American Machinist, April 1973, page 45.

20. McIntosh, R. et al. "The International Heat Pipe Experiment," AIAA Paper No. 75-726, May 1975.

21. Suelau, H. J. and Brennan, P. J. "Thermal Design of TIROS-N Heat Pipe Experiment Package (HEPP)," BK018-1024, B & K Engineering, Inc. February 1977.

22. Harwell, W. "Analysis and Tests of NASA Covert Groove Heat Pipe," NASA CR-135156, December 1976.

23. B & K Engineering "Summary Report for Effects of Non-Condensible Gas on Axially Grooved Heat Pipe Performance," June 1977.

24. Frank, S., et al. Heat Pipe Design Manual, Martin Marietta Corp., February 1967.

25. Hufschmidt, E. et al. "The Shearing Effect of Vapor Flow on Laminar Liquid Flow in Capillaries of Heat Pipes," NASA TT-F-16601, October 1975.

26. Chi, S. W. "Mathematical Modeling of Cryogenic Heat Pipes," NASA CR-116175, September 1970.

27. Schneider, G. E. and Yovanovich, M. "Thermal Analysis of Trapezoidal Grooved Heat Pipe Walls," University of Waterloo, August 1975.

28. Dynatherm Corporation, "Summary Report for Fill Determination Study of ATS-F & G Heat Pipes," December 1972.

29. Kamotani, Y. "Thermal Analysis of Axially Grooved Heat Pipes," 2nd International Heat Pipe Conference, April 1976.

30. Kamotani, Y. "Analysis of Axially Grooved Heat Pipe Condensers," AIAA Paper No. 76-147.

31. Molt, M. "Investigation of Capillary Forces and Surface Tension," 2nd International Heat Pipe Conference, April 1976.

32. Dynatherm Corporation, Heat Pipe Design Handbook, DRL-2, DRD No. SE-354T, NASA Contract No. NAS9-11927, August 1972.

APPENDIX A

DERIVATION OF EQUATIONS FOR PUDDLE FLOW

This appendix defines the analytical model which was developed to predict the performance of axially grooved heat pipes with puddle flow. When an axially grooved heat pipe is operated with excess working-fluid and in a gravity field, a puddle will form in the condenser end of the heat pipe. The driving force for liquid return in the puddle is provided by a gravity head developed by the elevation variation of the free surface of the puddle. Beyond the puddle, flow in the grooves is maintained by capillary pumping. The elevation head must support the viscous losses of the liquid mass flowing in the puddle. In addition, mass flow continuity between the puddle and the grooves extending beyond the puddle must be maintained. The following Eqs. were derived for puddle flow in an axial grooved heat pipe.

A-1 Equation of Motion in the Puddle.

Assuming one-dimensional flow in the puddle, a force balance on a fluid element as shown in Fig. 3-6 results in the following equation:

$$\rho_\ell g \, \mathrm{Cos}\beta \, \frac{dh_p}{dx} = \rho_\ell g \mathrm{Sin}\beta + \left(\frac{dp}{dx}\right)_{p\ell} \qquad \text{(A-1)}$$

The liquid pressure drop is assumed to be given by the Hagen-Poiseuille theory for laminar flow.

$$\left(\frac{dp}{dx}\right)_{p\ell} = \frac{\mu_\ell \, m_p}{(KA)_p \rho_\ell} \qquad \text{(A-2)}$$

where

$$K_p = \frac{16}{2(fRe)} \left(\frac{A_p}{WP_p}\right)^2 \qquad \text{(A-3)}$$

$$A_p = R_v^2 \left\{\frac{\theta_p}{2} - \frac{1}{2}\,\mathrm{Sin}\theta_p\right\} + A_\ell \frac{N}{2\pi}\theta_p \qquad \text{(A-4)}$$

$$WP_p = WP_\ell \frac{N}{2\pi}\theta_p \qquad \text{(A-5)}$$

$$h_p = R_v \left\{1 - \mathrm{Cos}\frac{\theta_p}{2}\right\} \qquad \text{(A-6)}$$

Substituting Eqs. (A-2) - (A-6) into (A-1) yields

$$\rho_\ell g \mathrm{Cos}\beta \frac{R_v}{2} \mathrm{Sin}\frac{\theta_p}{2} \frac{d\theta_p}{dx} = + \rho_\ell g \mathrm{Sin}\beta - \frac{\mu_\ell m_p}{(KA)_p \rho_\ell} \qquad \text{(A-7)}$$

A-2 Continuity Equation

When the puddle flows from stations X + Δ X and X in Fig. 2-6 some of the liquid mass is leaving the puddle and flowing into the groove at the interface to satisfy the condition of mass continuity. If the element is located in the condenser section and uniform axial condensation is assumed, there is liquid mass flowing into the puddle element. Therefore, a mass flow balance for the element will yield

$$dm_p = dm_g - dm_c \qquad \text{(A-8)}$$

where $dm_c = 0$ for the element located in the adiabatic section, and in the evaporator $dm_c = - dm_e$. From the first law of thermodynamics one can directly relate the mass flow to the axial heat flow rate, i.e.

$$m_p = - \frac{Q_p}{\lambda} \qquad \text{(A-9)}$$

Therefore, in the future analysis, one may utilize the axial heat flow rate Q_p and the maximum heat transport Q_m for the determination of dm_g, dm_c, dm, and dm_e. The term dm_g can be obtained from the analysis of the region extending beyond the puddle where the capillary pumping flow prevails. In order to reduce the complexity of the mathematical model for the capillary pumping flow, one can utilize results from the closed form solution. The closed form solution has shown that the maximum heat transport at ideal charge can be approximately expressed as:

$$Q_m = Q_{mo}\left(1 - \frac{h_s}{h_{max}}\right) \tag{A-10}$$

where Q_{mo} is the maximum heat transport at the zero elevation and ideal charge, and h_s is the static elevation of the heat pipe. For a heat pipe with a puddle h_s becomes the static elevation of a given groove above the puddle. For the groove i of Figure 3-6 one has

$$h_s = \beta X \tag{A-11}$$

Since the partially submerged groove has a shorter length where the capillary pumping flow prevails, one must formulate Q_{mo} to take this effect into consideration. The closed form solution of the liquid flow analysis also showed that Q_{mo} could be written as

$$Q_{mo} = \frac{(QL)_{max}}{L_{eff}} \tag{A-12}$$

where

$$(QL)_{max} = \int_o^L Q(X)dX$$

for the grooves unaffected by the puddle. Because the effects of the vapor viscous loss and liquid-vapor shear loss do not change the general behavior of the heat pipe, one can assume that Eq. (A-12) is still valid for the case including these effects. $(QL)_{max}$ can then be obtained from the computer program for ideal charge and zero elevation. When Eq. (A-12) is applied

to the i th groove of Figure 3-6, L_{eff} is replaced by X_{eff} which is a function of X, L_e, L_a and L_c. The element located in the condenser has

$$X_{eff} = (X - L_e - L_a) \left\{ 1 - \frac{1}{2 L_c} (X - L_a - L_e) \right\} + L_a + \frac{1}{2} L_e \quad \text{(A-13a)}$$

and the element located in the adiabatic section

$$X_{eff} = X - \frac{1}{2} L_e \quad \text{(A-13b)}$$

if located in the evaporator

$$X_{eff} = \frac{X}{2} \quad \text{(A-13c)}$$

It should be noted that Q_m in Equation (A-10) is the maximum heat transport. If a uniform heat output is assumed for the i th groove, the heat output (i.e. mass condensation) between $(L_e + L_a)$ and X should be considered. Therefore, combining Equations (A-9) - (A-13) and the effect of heat removal between $(L_e + L_a)$ and X, one has

$$dm_g = \frac{(QL)_{max}\, d\theta_p}{2\pi\lambda\, X_{eff}} \left(1 - \beta \frac{X}{h_{max}}\right) \left\{ 1 - \frac{1}{L_c} (X - L_e - L_a) \right\} \quad \text{(A-14a)}$$

where

$$L_e + L_a \leq X \leq L_a + L_e + L_c$$

similarly

$$dm_g = \frac{(QL)_{max}\, d\theta_p}{2\pi\lambda\, X_{eff}} \left(1 - \beta \frac{X}{h_{max}}\right) \frac{X}{L_e} \qquad \text{for } 0 \leq X \leq L_e \quad \text{(A-14b)}$$

and

$$dm_g = \frac{(QL)_{max}\, d\theta_p}{2\pi\lambda\, X_{eff}} \left(1 - \beta \frac{X}{h_{max}}\right) \qquad \text{for } L_e \leq X \leq L_a + L_e \quad \text{(A-14c)}$$

One now turns to the determination of dm_c and dm_e. For uniform condensation in the condenser one can write

$$dm_c = \frac{Q_{sp}}{\lambda L_c} dx \tag{A-15}$$

where

$$Q_{sp} = \int_0^{\theta} \frac{(QL)_{max}}{2\pi X_{eff}} \left(1 - \beta \frac{X}{h_{max}}\right) d\theta_p \tag{A-16}$$

and Q_{sp} is the heat capacity transported by the grooves affected by the puddle.

Equation (A-16a) can be rewritten in a differential form

$$\frac{dQ_{sp}}{dX} = \frac{(QL)_{max}}{2\pi X_{eff}} \left(1 - \beta \frac{X}{h_{max}}\right) \frac{d\theta_p}{dX} \tag{A-16a}$$

For uniform evaporation in the evaporator, one has

$$dm_e = \frac{Q_{sp}}{\lambda L_e} dX \tag{A-17}$$

Substituting Equations (A-14) - (A-17) into Equation (A-8) one has

(1) In the condenser, $L_e + L_a \leq X \leq L_e + L_a + L_c$

$$\frac{dQ_p}{dX} = \frac{(QL)_{max}}{2\pi X_{eff}} \left(1 - \beta \frac{X}{h_{max}}\right) \left\{1 - \frac{1}{L_c}(X - L_e - L_a)\right\} \frac{d\theta_p}{dX} - \frac{Q_{sp}}{L_c} \tag{A-18a}$$

$$\frac{dQ_{sp}}{dX} = \frac{(QL)_{max}}{2\pi X_{eff}} \left(1 - \beta \frac{X}{h_{max}}\right) \frac{d\theta_p}{dX} \tag{A-19a}$$

where

$$X_{eff} = (X - L_e - L_a)\left\{1 - \frac{1}{2\,L_c}(X - L_a - L_e)\right\} + L_a + \frac{1}{2}L_e$$

(2) In the adiabatic section, $L_e \leq X \leq L_e + L_a$

$$\frac{dQ_p}{dX} = \frac{(QL)_{max}}{2\pi\ X_{eff}}\left(1 - \beta\ \frac{X}{h_{max}}\right)\ \frac{d\theta_p}{dX} \qquad \text{(A-18b)}$$

$$\frac{dQ_{sp}}{dX} = \frac{(QL)_{max}}{2\pi\ X_{eff}}\left(1-\beta\ \frac{X}{h_{max}}\right)\frac{d\theta_p}{dX} \qquad \text{(A-19b)}$$

where

$$X_{eff} = X - \frac{1}{2}L_e$$

(3) In the evaporator, $0 \leq X \leq L_e$

$$\frac{dQ_p}{dX} = \frac{(QL)_{max}}{2\pi\ X_{eff}}\left(1 - \beta\ \frac{X}{h_{max}}\right)\frac{X}{L_e}\ \frac{d\theta_p}{dX} + \frac{Q_{sp}}{L_e} \qquad \text{(A-18c)}$$

$$\frac{dQ_{sp}}{dX} = \frac{(QL)_{max}}{2\pi\ X_{eff}}\left(1 - \beta\ \frac{X}{h_{max}}\right)\frac{d\theta_p}{dX} \qquad \text{(A-19c)}$$

where

$$X_{eff} = \frac{1}{2}X$$

APPENDIX B

EMPERICAL EQUATION FOR CAPILLARY PUMPING LIMIT

The governing equation for the capillary pumping limit with laminar flow in an axially grooved heat pipe (i.e. Eq. 2-18) can be written as:

$$\frac{\sigma}{R_x^2}\frac{dR_x}{dX} - \rho_\ell \mathrm{Sin}\beta = \frac{\nu_\ell}{K_x A_{\ell x}}\left[1 + 8\frac{\nu_v}{\nu_\ell}\frac{K_x A_{\ell x}}{A_v R_v^2} + \frac{\phi^2}{3}\psi\right]\frac{Q_x}{\lambda} \qquad \text{(B-1)}$$

The vapor flow characteristic ($A_v R_v^2$) is a constant at any axial location along the length of the heat pipe while the liquid flow conductance ($K_x A_\ell$) is a function of meniscus recession which is dependent on the axial location X. Rewriting equation (B-1) and integrating it from the upstream end of the evaporator to the downstream end of the condenser gives

$$\frac{\sigma\lambda}{\nu_\ell}\left\{\int_{1/2w}^{\infty}\frac{K_x A_{\ell x}}{R_x^2}dR_x - \int_0^L \frac{\rho_\ell g \,\mathrm{Sin}\beta (K_x A_{\ell x})}{\sigma}dX\right\}$$

$$= \int_0^L \left(1 + 8\frac{\nu_v}{\nu_\ell}\frac{K_x A_{\ell x}}{A_v R_v^2} + \frac{\phi^2}{3}\psi\right)Q_x dX \qquad \text{(B-2)}$$

The first term on the left hand side of equation (B-2) represents the liquid flow and pumping characteristic which is a function of the groove form and is dependent solely on groove properties and meniscus recession. The properties of any groove form can be defined by a flow factor N_g as follows:

$$NN_g = \int_{1/2w}^{\infty}\frac{K_x A_{\ell x}}{R_x^2}dR_x \qquad \text{(B-3)}$$

Where N is the total number of grooves in the heat pipe.

The second term on the left hand side of Eq. (B-2) represents the gravity loss. This term can be integrated if an average value for $K_x A_{\ell x}$ as defined:

$$\overline{KA_\ell} \equiv \frac{1}{L}\int_o^L K_x A_{\ell x}\, dX \tag{B-4}$$

The second term of equation (B-2) then becomes:

$$\int_o^L \frac{\rho_\ell g \sin\beta}{\sigma} (K_x A_{\ell x}) dx = \frac{\rho_\ell g \sin\beta}{\sigma} \overline{KA}_\ell L \tag{B-5}$$

An evaluation of the results from the GAP program indicates that $\overline{KA}_\ell$ can be taken to be approximately equal to $NN_g \frac{W}{2}$. It should be noted that this approximation does not apply to convergent (triangular) grooves because the integration limit of Eq. (B-3) is restricted to ½W, whereas the integration limit for a convergent groove is defined by the root dimension of the groove. Eq. (B-3) can then be rewritten for divergent grooves as:

$$NN_g = \frac{2\overline{KA}_\ell}{W} \tag{B-6}$$

And Eq. (B-5) becomes:

$$\int_o^L \frac{\rho_\ell g \sin\beta}{\sigma} (K_x A_{\ell x}) dX = \frac{\rho_\ell L \sin\beta}{\sigma} \frac{NN_g W}{2} \tag{B-7}$$

On the basis of exact solutions obtained with the GAP computer program it was determined that the average liquid flow conductance can also be used to simplify the integration of the right hand side of Eq. (B-2). Referring

to Fig. 3-1, the axial heat flow rate Q_x can be expressed in terms of total heat input Q for each of the heat pipe regions:

$$\begin{aligned}
&\text{Evaporator:} && 0 < X < L_e && , Q_x = \frac{QX}{L_e} \\
&\text{Adiabatic:} && L_e < X < L_e + L_a && , Q_x = Q \\
&\text{Condenser:} && L-L_c < X < L && , Q_x = \frac{Q(L-X)}{L_c}
\end{aligned} \qquad \text{(B-8)}$$

The integral of the right hand side of Eq. (B-2) becomes:

$$\int_0^L \left(1 + 8 \frac{\nu_v}{\nu_\ell} \frac{K_x A_{\ell x}}{A_v R_v^2} + \frac{\phi^2}{3} \psi\right) Q_x dX$$

$$= \left(1 + 4 \frac{\nu_v}{\nu_\ell} \frac{NN_g W}{A_v R_v^2} \frac{\phi^2}{3} \psi\right) QL_{eff} \qquad \text{(B-9)}$$

Combining Eqs. (B-2), (B-3), (B-6), (B-8), and (B-9) yields the following relationship:

$$\frac{QL_{eff}}{N_L} = \frac{NN_a \left\{1 - \frac{h}{H} \frac{W}{2}\right\}}{\left\{1 + \frac{\nu_v}{\nu_\ell} (f_v + f_{\ell v})\right\}} \qquad \text{(B-10)}$$

where $L_{eff} = \frac{1}{2} L_e + L_a + \frac{1}{2} L_c$

$$h = L \sin\beta$$

$$NN_g = \int_{1/2w}^{\infty} \frac{K_x A_{\ell x}}{R_x^2} dR_x$$

$$f_v = \frac{4}{\pi} \frac{NN_g W}{R_v^4} = \frac{4}{\pi} \frac{NN_g}{\left(\frac{R_i}{W} - \alpha\right)^4 W^3}$$

$$f_{\ell v} = \frac{1}{3\alpha} \frac{N}{\pi} \frac{A'_\ell}{R_v^3} = \frac{1}{3\alpha} \frac{N}{\pi} \frac{A'_\ell}{W^2} \frac{1}{\left(\frac{R_i}{W} - \alpha\right)^3}$$

with

A_ℓ = Area of a single groove with no meniscus recession.